An investigation into Sunitinib malate nanoparticle production by US- RESOLV method: Effect of type of polymer on dissolution rate and particle size distribution

Fariba Razmimanesh[a,b,c], Gholamhossein Sodeifian[a,b,c,*], Seyed Ali Sajadian[a,b,c]

[a] Department of Chemical Engineering, Faculty of Engineering, University of Kashan, 87317-53153 Kashan, Iran
[b] Laboratory of Supercriritcal Fluids and Nanotechnology, University of Kashan, 87317-53153 Kashan, Iran
[c] Modeling and Simulation Centre, Faculty of Engineering, University of Kashan, 87317-53153 Kashan, Iran

HIGHLIGHTS

- The US-RESOLV method was applied to produce Sunitinib malate nanoparticles for the first time.
- Process parameters were optimized based on morphology, size distribution, and dissolution rate of produced particles.
- Four polymers were useful for modifying the size distribution and increasing the dissolution rate of nanoparticles.
- The combined effects of the smaller particle size, *ultrasonication* and polymers presence could enhance dissolution rate.

GRAPHICAL ABSTRACT
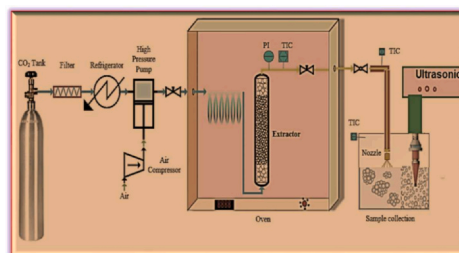
ABSTRACT

The present study practiced ultrasonic-assisted rapid expansion of a supercritical CO$_2$ solution into a liquid solvent (US-RESOLV) process for the synthesis of nanoparticles (NPs) of Sunitinib malate for the first time. Hydrophilic polymers including hydroxypropyl methylcellulose (HPMC), poly (vinyl alcohol) (PVA), chitosan (CHI) and polyethylene glycol (PEG) were utilized for modifying the size distribution and increasing the dissolution rate of the Sunitinib malate NPs. Also, we determined the impact of pressure, nozzle diameter as well as temperature on morphology, size distribution and dissolution rate of produced particles. In order to accomplish the objectives of the present study, PEG was the best polymer for controlling the particle size distribution and HPMC served as the best polymeric stabilizer for increasing the dissolution rate of the drug particles. The

synthesized particles were much smaller (< 600 nm) in comparison to the unprocessed particles of Sunitinib malate. The combined effects of the smaller sizes of the particles, ultrasonication and the presence of polymers could enhance dissolution rate of the Sunitinib malate in the aqueous media.

1. Introduction

Sunitinib as a novel vascular endothelial growth factor receptor inhibitor, has presented high activity in renal cell carcinoma (RCC) and is now extensively applied for patients with metastatic disease [1]. It is the new small molecularly targeted anti-cancer medicine with the survival merits in the advanced renal cell carcinoma and in the advanced hepato-cellular carcinoma and gastro-intestinal stromal tumors, respectively [2–4].

Moreover, Sunitinib malate has been proposed to be an orange-to-yellowish solid with a molecular formula $C_{26}H_{33}FN_4O_7$ with the molecular weight equal to 532.56 g/mole. This solid could be solved in dimethyl sulfoxide at 40 mg mL^{-1} but it very poorly soluble in water and ethanol [5]. In addition, it can be solved in acidic aqueous solutions (25 mg mL^{-1} at the pH of 1.2–6.8). The solubility of this medicine quickly diminishes at the pH values > 6.8 (water solubility"1 mg mL^{-1}) [6]. Once used orally, the Sunitinib is known to follow a slow absorption stage throughout the gastrointestinal tract while its concentration in the plasma reaches a maximum within 6–12 h [5]. One of the prominent goals of developing solid-state drug has been considered to be enhance the medicine solubility with maintenance of its stability. Such a goal will be essential as permeability as well as solubility have been introduced as two main parameters applied to explain the oral adsorption based on the bio-pharmaceutics classification system (BCS). Recently, particle size reduction has been applied in the pharmaceutical industry to modify specifications of the solid forms including solubility, stability, dissolution rate and bioavailability without altering the desired effect of drug [7–9]. Nanosuspensions refer to mixes where solid nanoparticles (NPs) of a drug are dispersed in a liquid and further stabilized by polymer and/or surfactant. The so-called Noyes–Whitney relationship implies that the API (active pharmaceutical ingredient) dissolution rate improves remarkably upon miniaturizing the particle size, thereby boosting the bioavailability of the NPs. There are also chances that the NPs get attached to the gastrointestinal mucosa; this tends to extend the transit time of the drug and hence contributes to its absorption [10].

Application of supercritical fluid (SCF) technology that is one of the options for reducing particle size of pharmaceutical compounds, has recently received a lot of attention. Experts in the field utilized this approach in the pharmaceutical and biochemical industries for improving the bioavailability of poorly water-soluble medicines by decreasing their particles size to the micro- and nano-scales. Earlier studies regarding the usage of SCF technologies to form the particles have considered the supercritical antisolvent (GAS, SAS, SEDS & ASES) as well as fast expansion of the supercritical solution (RESOLV, RESS, RESS-SC & RESSAS) methods which have been widely investigated [11–24].

RESS (rapid expansion of supercritical solution) has been used as a cost-effective, innovative and promising process for preparing nano- and sub-micron pharmaceutical particles that have high-solubility in supercritical CO_2 (SC-CO_2) with narrow size distribution in solvent-free condition [25,26]. The basic principle of this process is the contrast in solute solubility in the SCF between high and low pressures. This method works by abruptly expanding the supercritical solution through some nozzle to achieve sonic velocities [27–29]. In this method, expansion and pre-expansion conditions as well as extraction variables including pressure, temperature, nozzle diameter, nature and presence of the cosolvent and spray distance affect particle size distribution [25,26,30]. Sun et al. [31–33] modified conventional RESS by using solution or a liquid solvent as a receptor (RESOLV) to expand the

supercritical solution into a liquid solvent instead of the ambient air [34]. Pharmaceutical particles generated via RESOLV (rapid expansion of a supercritical CO_2 solution into a liquid solvent) are smaller in comparison to the ones observed by RESS because the application of a liquid as the receptor in the rapid expansion phase can prevent coagulation and condensation in the expansion jet, therefore efficiently inhibit fast procedure of the particles' growth [35]. RESOLV technique was applied for minimization of the particles' aggregation in the course of the jet expansion. For this purpose, the supercritical solution has its pressure dropped by being introduced, via an orifice into a collection chamber that was pre-loaded by an aqueous fluid at ambient temperature. The resultant suspension of NPs was stabilized by adding different water-soluble polymers/surfactants to the mixture [35]. Although the particle size is utilized as a critical parameter involving in the medicine performance in many cases, it is most often very difficult to achieve a uniform particle size distribution.
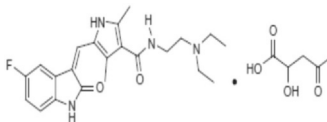
According to previous researches, it has found out that polymers (PVP, HPMC, PVA, PEG, etc.) have received much attention in this field [33,36–40]. A number of investigators confirmed probable use of RESOLV to nano-size the water-insoluble medicines in the aqueous suspensions [33,37,41–45]. The drugs are delivered at a predetermined rate by designing the controlled release systems. In addition, mean size, morphology, distribution of the particle size, distribution of the pore size, polarity as well as the molecular weight of polymers may affect the ways of releasing drugs. Choosing a proper polymer for dispersion of pharmaceutical compounds is considered as a challenge. The polymers used as carriers should have some features such as biocompatibility and biodegradability [46,47]. Upon exposure to the aqueous medium encountered in the gastrointestinal tract, a solid dispersion of a drug is known to turn into a supersaturated drug solution. Under such circumstances, the drug particles tend to get precipitated rather than being appropriately absorbed by the respective cells, leading to attenuated bioavailability of the drug. As a workaround, studies have been performed with different polymer excipients to extend the time of the supersaturation and hence retard the precipitation of the drug particles. In the other words, the polymer must be capable of retaining a drug at supersaturated concentration for long enough to enable proper absorption of the drug particles [48]. In this research, hydroxypropyl methylcellulose (HPMC) [48–51], poly (vinyl alcohol) (PVA) [46,50], chitosan (CHI) [50–54] and polyethylene glycol (PEG) [55,56] polymers were applied as stabilization agents because of their useful features.

Despite the benefits of polymers in RESOLV process, there are chances that the NPs of drug and/or polymer agglomerate upon exposure to the receptor solution. Indeed, the main difficulties with the RESOLV method include the particle agglomeration and the resultant non-uniform particle distribution. In the previous research [57], for the first time, ultrasonication method was considered to dominate particle agglomeration and the obtained results showed that application of ultrasonication is effective in reducing particle size and homogenization.

The ultrasonication process generates sound waves by inducing pressure changes in the aqueous medium. This builds so-called gas pockets that nucleate some microbubbles. It takes only microseconds for the microbubbles to nucleate, grow and finally burst, with the eventual result being high-temperature and pressure micro-implosions [58,59]. Moreover, ultrasonic irradiation compels the pressure waves, which provide cavity. Therefore, the mentioned technique is considered as a powerful technique for homogenization and particle size reduction in different fields of nanotechnology [57,60,61].

During twenty past years, the micro- as well as nano-sized medicine as well as the polymer particles were produced by the RESOLV method.

Table 1
Molecular structure and physicochemical properties of Sunitinib malate.

Compound	Formula	Structure	M_W (g/mol)	λ_{max} (nm)	CAS number	Mass fraction purity (Analysis method)
Sunitinib malate	$C_{26}H_{33}FN_4O_7$		532.56	440	341031-54-7	99% (HPLC method)
Carbon dioxide	CO_2		44.01		124-38-9	99.8% (GC method)

Pathak et al. [62] investigated the application of RESOLV technique for preparing the antiparasitic drug (Amphotericin B) NPs. The well-dispersed Amphotericin B NPs suspended in a stable aqueous solution were produced, also suspension was additionally stabilized in the presence of the water-soluble polymers.

Meziani et al. [63] prepared nanocrystalline silver particles using SCF technique RESOLV with chemical reduction. They used poly(*N*-vinyl-2-pyrrolidone) (PVP) or BSA (bovine serum albumin) protein as a protecting agent for suspension of nano-particle. Results showed that the BSA protein protected Ag NPs are much larger than the ones prepared by PVP. Xiang et al. [64] fabricated gambogic acid NPs by using RESOLV method for enhancing medicine solubility in water. Therefore, the produced gambogic acid NPs by RESOLV technique, were investigated and the obtained results showed that RESOLV procedure can substantially produce nano-suspension of gambogic acid with the greater bioavailability as well as anti-neoplastic efficiency and these NPs can possess many potentials in the drug field.

Sodeifian and Sajadian [57] applied the RESOLV, US-RESOLV as well as RESS processes to provide nano sized amiodarone hydrochloride (AMH). PVP and HPMC polymers were considered for stabilization and controlling sizes of AMH NPs. They concluded that usage of polymer couple with ultrasonic waves enhance the rate of dissolution of AMH in the aqueous solutions more than just polymer.

The present research is the first for using ultrasonic-assisted RESOLV (US-RESOLV) method for controlling the size and size distribution of Sunitinib malate as an anticancer drug. HPMC, PVA, CHI and PEG polymers were considered as stabilization agents and their influences on the features of the generated Sunitinib malate micro and nanoparticles were evaluated. The US-RESOLV-assisted Sunitinib malate particles were investigated by a variety of physical characterization methods including Dynamic Light Scattering (DLS), Field Emission Scanning Electron Microscopy (FESEM), X-ray Diffraction (XRD),

Fourier Transform Infrared (FTIR) analyses as well as Differential Scanning Calorimetry (DSC), and compared to the unprocessed Sunitinib malate. Also, the impacts of pressure, nozzle diameter and temperature on morphology, size distribution and dissolution rate of resultant micro and nanoparticles were studied and optimized via Taguchi methodology.

2. Material and methods

2.1. Materials

According to the research design, Sunitinib malate (CAS Number 341031-54-7, purity > 99%) and carbon dioxide (CO_2) (CAS Number 124-38-9, purity > 99.99%) were procured from Parsian Pharmaceutical as well as Fadak Companies (Iran), respectively, and employed as received (Table 1). HPMC 4000 cPs (HPMC K4M), PVA (molecular weight 145,000), CHI (medium molecular weight, 85% deacetylated) and PEG (Average molecular mass: 28,000–38,000) were provided by Sigma Aldrich (Germany).

2.2. Methods

2.2.1. Ultrasonic-assisted RESOLV apparatus and procedure (US-RESOLV)

Fig. 1 shows applied US-RESOLV apparatus in this research. As it is observed, this system was the same as the RESS apparatus, with the only difference being the fact that a liquid solution-loaded chamber hosted the rapid expansion in the US-RESOLV apparatus used in this work. The system consisted of two main sections, including RESOLV and ultrasonication parts. At first, the extraction cell was loaded with 2 g of Sunitinib malate couple with glass beads with a diameter of 2 mm to avoid channeling and enhance drug-carbon dioxide contact surfaces. Furthermore, 2 sintered filters have been placed over the two ends of
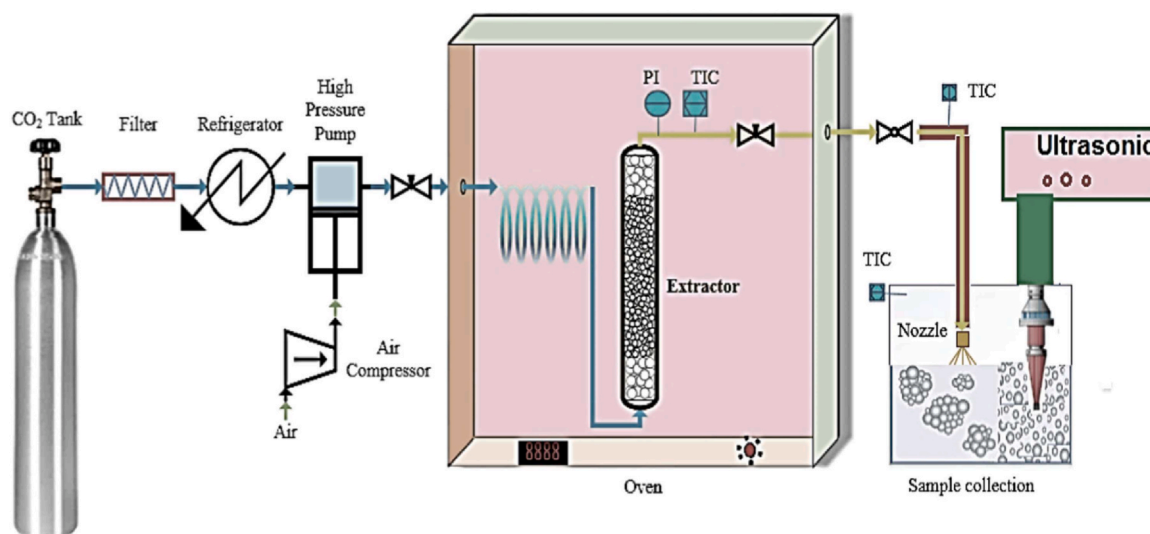

Fig. 1. The experimental equipment of US-RESOLV method.

the cell to hold the undissolved solute within the extractor. In the beginning of the process, a refrigerator was used to decrease the temperature of carbon dioxide to around 253 K in an attempt not to have the CO_2 gas formed within the piston and hence keep the high-pressure pump from being gas locked. Then, the reciprocating high pressure pump injected carbon dioxide into the 70-mL extraction cell until proper pressure was achieved (up to 600 bar). The desired temperatures were adjusted with an exactly temperature controlled oven with an accuracy of ± 0.1 K. A static time 120 min has been considered to achieve the equilibrium state and after, the saturated Sunitinib malate-CO_2 solution was injected into a capillary nozzle via a preheated, 1/8" stain-less steel tube and a fine needle valve. This was done to keep the nozzle open in the course of the expansion stage. Moreover, fast expansion has been performed upon introduction of the solution, via the nozzle, into a polymer-loaded container (1% w/v) that was further equipped with an ultrasonication unit. The ultrasonication was done by a probe of 13 mm in diameter that operated at 20 kHz to generate the output power equal to 70 W. The procedure has been completely explained in our previous papers [17,21,27].

2.2.2. Characterization methods

DSC, XRD, DLS, FTIR and FESEM analyses were used to investigate the Sunitinib malate particles. The DSC analysis (DSC 404 F3 Pegasus; Netzsch Company: Germany) provided us with the melting points of the original and processed drug species. This was done by heating some 5 mg of the sample from 30 to 200 °C at 10 °C/min in a standard aluminum pan in an atmosphere of argon flowing at 20 mL/min. On a Philips X'pert Pro MPD X-ray diffracto-meter, XRD patterns of the original and treated APIs were recorded by means of Cu-Kα radiation (λ = 0.154 nm) at ambient temperature at different 2θ values in the ranges from 5° to 80°.

FTIR analysis results provided us with absorption spectra. To this end, 4 mg of Sunitinib malate was coupled with spectral-grade potassium bromide (300-mg KBr) by means of mortar and pestle, and the result was subjected to pressing to obtain a test-ready KBr disk. Conducted on a Hitachi S-4160 FESEM apparatus operating at 20 kV, the FESEM analysis results were devised to evaluate the particles in terms of morphology, i.e. geometry and surface properties. FESEM samples were prepared by sputter-coating the drug powder with gold–palladium alloy. For the sake of RESOLV imaging, a few drops of the nanoparticle-suspended mixture were put on a carbon tape and the tape was dried under ambient conditions. The DLS analysis was done to see the particle size distribution. The analysis was undertaken on a NANO-PHOX particle sizer (Sympatec GmbH System Partikel Technik) that has been equipped with a He-Ne laser with the wave-length equal to 623 nm and power of 10 mW), as a light source, that operated at 90° scattering angle. Prior to DLS analysis, some 0.01 g of Sunitinib malate was dissolved in 10 mL of deionized water.

2.2.3. Dissolution rate

A phosphate buffer solution (PBS) with a pH of 7.4 has been utilized to see how are the dissolution rates of the unprocessed and processed Sunitinib malate particles affected by the particle size and morphology. Tests were performed in a 100-mL vessel wherein the dissolution medium temperature and stirring rate were adjusted to 310 ± 0.5 K and 100 rpm, respectively [65,66]. As a first step, 30 mg of the Sunitinib malate was introduced into 100 mL of the dissolution medium. Then, a 450-nm syringe filter was utilized to take 3 mL of the liquid sample following 5, 10, 15, 30, 60, 90 as well as 120 min, and an equal volume of the fresh PBS has been poured into vessel to keep the total volume unchanged. Next, UV–vis spectro-photometry (GBC Scientific Equipment Ltd, Cintra-101) has been conducted at 440 nm to evaluate the dissolved amount of the drug in the considered sample. The experiments have been accomplished three times and then the average values were determined.

2.2.4. Experimental design of the process parameters

The so-called Taguchi method is a well-known approach to the design of experiments (DoE) for determining optimal values of the parameters for a particular process. In this work, the DoE was practiced on the RESOLV process with four orthogonal parameters at four levels (L16 (4^4)), which were selected according to the results of a set of preliminary tests.

3. Result and discussion

We measured experimental solubility of Sunitinib malate at various conditions of temperature and pressure in our previous study [67]. The obtained results (mole fractions ranged between 0.5×10^{-5} and 8.56×10^{-5}) indicated that US-RESOLV can be the desirable approach to form micro and nanoparticles of Sunitinb malate. Numerous parameters can affect particle size, particle size uniformity, morphology and dissolution rate of the pharmaceutical compounds in the US-RESOLV method; these parameters include temperature, pressure, nozzle diameter, type of used polymer, nozzle length, spray distance, co-solvent content and flow rate. The present study analyzed the impacts of temperature (308–338 K), pressure (180–270 bar), diameter of nozzle (150–450 μm) and type of applied polymer (HPMC, PVA, CHI and PEG) on the particle size uniformity, dissolution rate and morphology of the Sunitinib malate particles with ultrasonic assistance. For this purpose, Taguchi methodology (L-16 orthogonal array) has been applied to investigate effects of mentioned variables on specifications of the produced particles. The obtained outputs were presented in Tables 2–4 and Figs. 2 and 4. To achieve more reliable results, all measurements were conducted in triplicate and average values of the size of particles, uniformity of particle size and dissolution rate have been reported.

3.1. Investigating the impacts of the operating variables on the particle size uniformity (SPAN value)

The SPAN (dispersion index) is a statistical value to investigate the particle size distribution and is obtained as follows:

$$SPAN = \frac{D_{90} - D_{10}}{D_{50}} \tag{1}$$

where D_{90}: diameter of particle, at which 90% of the population resides are under the point D_{90}.

D_{10}: diameter of particle, at which 10% of the population resides are under the point D_{10}.

D_{50}: diameter of particle, at which 50% of the population resides are above this point and 50% of the resides are under this point [10,68]. The relatively smaller value of SPAN indicates the uniformity and narrow distribution of the particle size [69,70]. The research works investigating the impact of SPAN values on aerosol generation have been most commonly focused on the lung deposition, indicating differences in the deposition behavior with changing the SPAN value at the same primary particle size. Indeed, one can use the SPAN values to evaluate the spray quality. In this respect, the higher the SPAN value, the higher would be the cohesiveness and surface tension and hence the lower would be the available energy for liquid dispersion, which can be translated as limited dispersion efficiency of the nasal device. Hence, for a defined nasal spray, it is necessary to choose a lower SPAN for optimizing its aerosol function [71].

Assuming no interaction among different variables, the process parameters were statistically optimized by implementing the Taguchi's DoE to achieve the best possible the response (here the Sunitinib malate particle size uniformity upon the US-RESOLV method).

Using the data presented in Table 2, the analysis of variance (ANOVA) has done to see how significant were the effects of temperature (308, 318, 328 and 338 K), pressure (180, 210, 240 and 270), diameter of nozzle (150, 250, 350 and 450 μm) and type of stabilizer polymer (HPMC, PVA, CHI and PEG) on the SPAN in the RESOLV

Table 2

Operation conditions of the US-RESOLV processes and quantitative results.

Sample	T (K)	P (MPa)	Diameter of nozzle (μm)	Polymer	Mean particle size (nm)	Particle size uniformity (SPAN)	Dissolution rate (at 120 min)	Predicted particle size uniformity (SPAN)	Predicted dissolution rate (at 120 min)
1	338	27	150	HPMC	858.32	0.4353	0.9430	0.4238	0.9453
2	308	18	150	CHI	2013.30	0.0943	0.8768	0.0898	0.9005
3	318	21	150	PEG	2157.85	0.0632	0.7380	0.0750	0.7082
4	328	24	150	PVA	586.84	0.0939	0.8888	0.0854	0.8927
5	308	24	350	HPMC	2029.44	0.4124	0.8431	0.4895	0.8134
6	328	27	250	CHI	1017.85	0.1918	0.8916	0.2277	0.8619
7	328	18	350	PEG	1557.16	0.0143	0.7340	0.0139	0.7012
8	308	21	250	PVA	713.44	0.3973	0.8710	0.3868	0.8733
9	338	18	450	PVA	767.10	0.0751	0.8403	0.0892	0.8132
10	318	27	350	PVA	560.93	0.4055	0.8424	0.3861	0.8661
11	318	24	450	CHI	1150.09	0.3352	0.8047	0.3263	0.8070
12	328	21	450	HPMC	1066.98	0.1222	0.5250	0.1164	0.5487
13	338	21	350	CHI	1927.08	0.2432	0.6104	0.2210	0.6142
14	338	24	250	PEG	906.71	0.1942	0.5478	0.1848	0.5614
15	308	27	450	PEG	843.26	0.0943	0.4910	0.0857	0.4930
16	318	18	250	HPMC	1287.64	0.5072	0.9321	0.4610	0.9359

method. The F-value was used as a measure to distinguish between the significant and insignificant factors. Recall that an ANOVA table can be merely interpreted within a range of values (levels) regarded for each variable. For each variable, the impact was assessed based on the mean response at each level [72]. Accordingly, the effects of the parameters for which the p-value was sufficiently small ($p < 0.05$) while F-value was considerably large were acknowledged as significant on the outcomes of the RESOLV process. By examining Table 3, it can be concluded that temperature ($p = 0.0161$), pressure ($p = 0.0236$), nozzle diameter ($p = 0.0384$) and type of polymer ($p = 0.0083$) parameters are significant terms in particle size uniformity. The p- and F-values reported in Table 3 show that type of polymer is the most effective parameter on the particle size uniformity. Also, various statistical criteria like the coefficient of determination (R^2), the predicted coefficient of determination ($R^2_{,pred.}$), adjusted coefficient of determination ($R^2_{,adj}$), coefficient of variation (C.V.) as well as adequate precision were calculated to see how significant was the model. Based on the results, the model was found to be adequate, as per a determination coefficient, R^2, a $R^2_{,adj}$, and a $R^2_{,pred}$ of 0.9880, 0.9399, and 0.8170, respectively. The obtained value of the adjusted R^2 showed that operating parameters (temperature, pressure, nozzle diameter, and type of polymer), could explain 0.9399 of the variance in the particle size uniformity. Adequate precision demonstrates the ration of signal-to-noise. It should be noted that the ratio > 4 will be acceptable and a relatively large value of the adequate precision (16.74; that is > 4) highlighted the very good ratio of signal to noise to navigate the design space, with a reliability of the experiments approved by the relatively small value of the coefficient variation; that is, CV = 13.10.

Examining Fig. 2a presents that 328 K is the optimum temperature for production of Sunitinib malate couple with polymer NPs with narrow size distribution. However, at a pressure of 180 bar, nozzle diameter of 150 μm and using PEG polymer as stabilizer, increasing temperature from 308 to 318 K increased SPAN value; while increasing the temperature between 318 and 328 K led to a significant decline in SPAN value.

According to Fig. 2b, at the temperature equal to 308 K, 150 μm nozzle diameter and using PEG polymer, the pressure and particle size distribution are directly proportional. As the pressure increased, the SPAN value increased. This indicated that pressure increment leads to wider particle size distribution. The impacts of pressure on Sunitinib malate solubility in SC-CO$_2$ was examined in our previous study [67]. The pressure was found to impose a significant effect on increasing the solubility, possibly due to the resultant increase in the solvating power of SC-CO$_2$ due to its greater density as well as solubility under higher pressures. Put differently, distribution of the particles size is influenced by concentration of drug in the solution. Size distribution of particles in the solution with lower concentration has been narrower in comparison to the distribution of the more concentrated solution [73].

Fig. 2c presents the effect of nozzle diameter on the SPAN value at 308 K with 240 bar pressure, and using PEG polymer. Tests were performed at various nozzle diameters, namely 150, 250, 350, and 450 μm. According to Fig. 2c, the lowest SPAN value (narrow particle size distribution) was observed with a 150 μm nozzle. When diameter of the nozzle increased from 150 to 250 μm, the significant increment in SPAN value was observed. Then, enhancing diameter of nozzle diameter from 250 to 350 μm led to the significant decrease in the SPAN value from 0.1822 to 0.0962. Further, the SPAN value decreased slightly with enlarging the nozzle diameter from 350 to 450 μm.

In this research, four polymers (HPMC, PVA, CHI and PEG) were considered as the stabilizer to evaluate their influence on the particle size distribution. It has been well acknowledged that the type of polymer affects the outcomes of RESOLV method significantly by managing morphology as well as size of micro or nanoparticles [57]. As observed in Fig. 2d, the type of polymer has the considerable impact on the management of the size distribution of prepared particles.

Table 3

The ANOVA analysis based on particle size uniformity (SPAN).

Source	Std. Dev.	R-square	Adjusted R-square	Predicted R-square	p-Value	PRESS (predicted residual sum of squares)
Model	0.24	0.9880	0.9399	0.8170	0.0149	4.75

Source	Sum of Squares	df	Mean Square	F- Value	Prob > F	
Model	13.71	12	1.14	20.54	0.0149	Significant
T	3.52	3	1.17	21.13	0.0161	Significant
P	2.69	3	0.9	16.11	0.0236	Significant
Diameter of nozzle	1.88	3	0.63	11.29	0.0384	Significant
Polymer	5.61	3	1.87	33.63	0.0083	Significant
Residual	0.17	3	0.056			
Cor. Total	13.87	15				

Table 4
The ANOVA analysis based on dissolution rate.

Source	Std. Dev.	R-square	Adjusted R-square	Predicted R-square	p-Value	PRESS (**predicted residual sum of squares**)
Model	0.044	0.9940	0.9701	0.8300	0.0053	0.17

Source	Sum of Squares	df	Mean Square	F- Value	Prob > F	
Model	0.98	12	0.081	41.59	0.0053	Significant
T	0.15	3	0.049	24.94	0.0127	Significant
P	0.066	3	0.022	11.31	0.0384	Significant
Diameter of nozzle	0.31	3	0.1	52.09	0.0044	Significant
Polymer	0.46	3	0.15	78.01	0.0024	Significant
Residual	5.867×10^{-3}	3	1.956×10^{-3}			
Cor. Total	0.98	15				

Among used polymers, PEG and HPMC had the narrowest and widest particle size distribution, respectively. In addition, the SPAN value corresponding to PVA was smaller than that of CHI polymer. The determined difference in distributing the particles' size is due to structural differences of considered polymers. According to the previous researches [74,75], it can be concluded that in general, HPMC produces a narrow pore size distribution with high pore sizes, whereas, CHI, PVA and especially PEG have a wide pore size distribution with small pore sizes. These results can be observed in the SEM images (Fig. 3).

Optimum process conditions have found that 328 K, a 180 bar pressure, a nozzle diameter of 150 μm, as well as PEG polymer as a stabilizer, under which set of conditions, a SPAN value of 0.0112 could be achieved.

3.2. Investigating the effect of operating parameters on the dissolution rate

To study whether particle size reduction by using US-RESOLV method could improve the bioavailability of Sunitinb malate, rate of dissolution of the Sunitinib malate particles prepared by US-RESOLV was evaluated and then compared to that of the unprocessed drug knowing the fact that dissolution rate provides a measure of bioavailability of drug.

Therefore, effects of the distribution of the particles' size and also the particles' shape on the dissolution efficiency have been studied in the several researches [76–78].

Fig. S1 presents the dissolution rate profiles of un-processed and processed drug particles via US-RESOLV (HPMC (sample 5), PVA
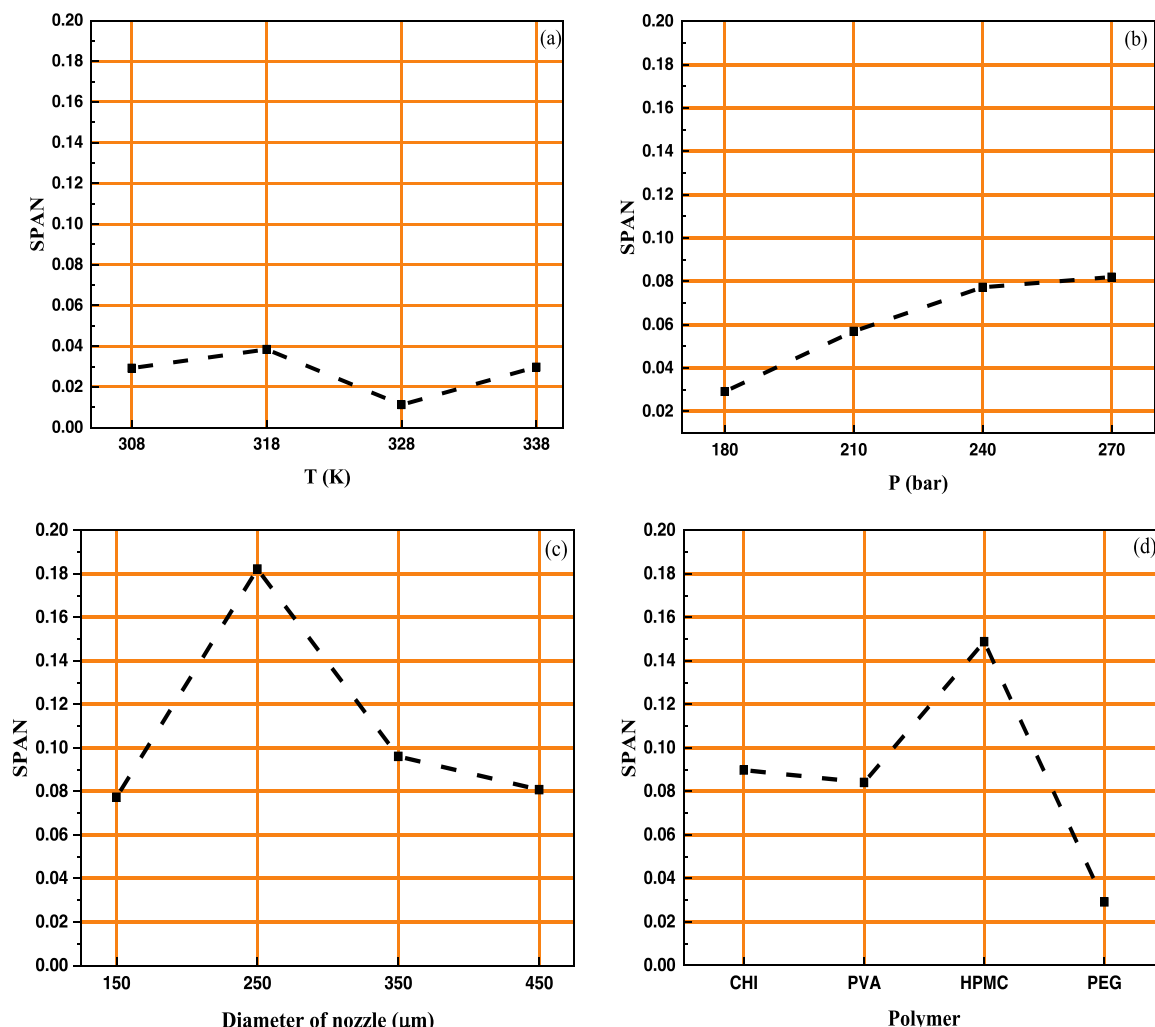

Fig. 2. The plot of the US-RESOLV procedure for SPAN value based on: (a) temperature (b) pressure; (c) nozzle diameter; (d) type of polymer.
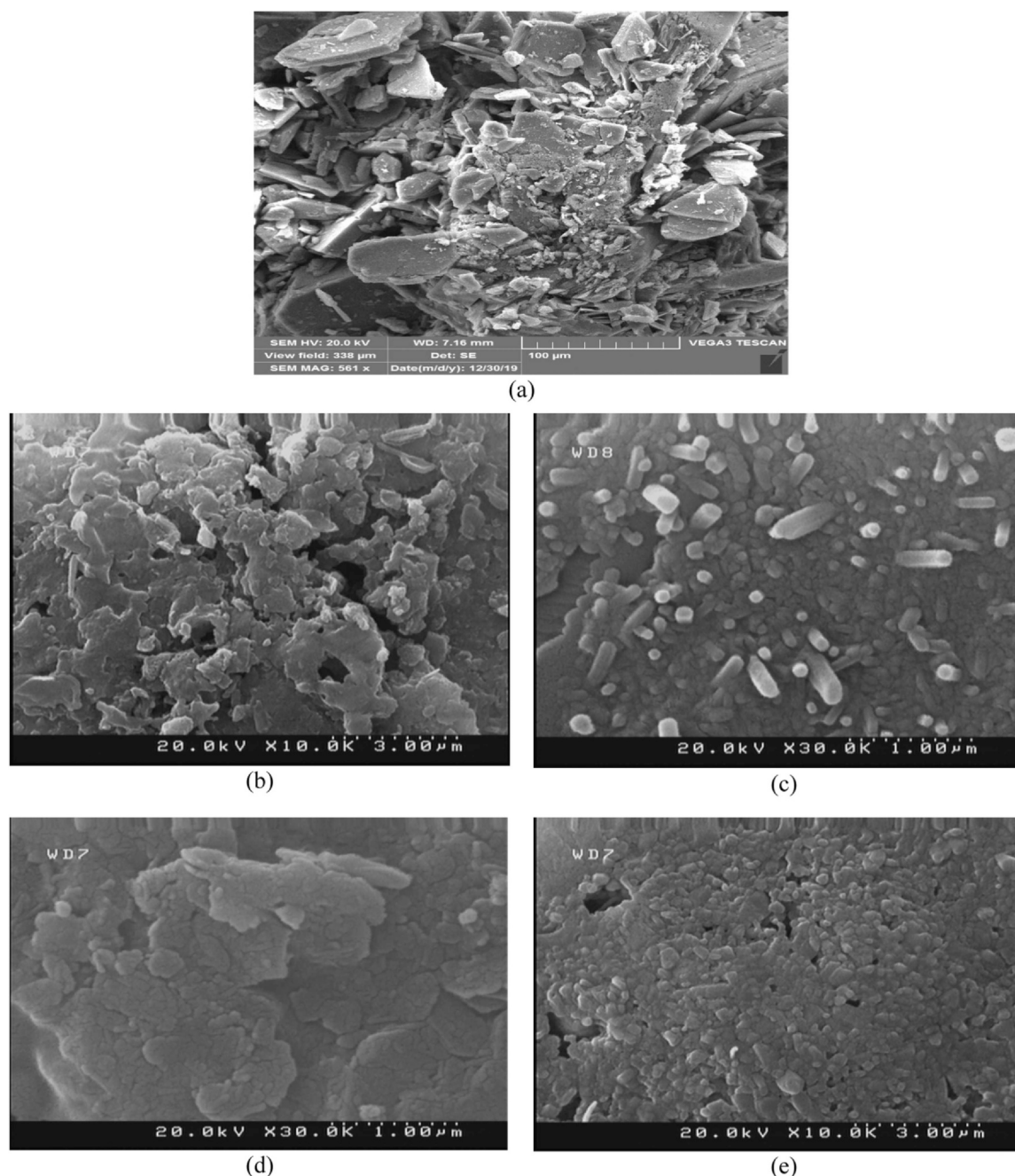
Fig. 3. SEM images of US-RESOLV method for different conditions: a) original Sunitinib malate, b) Sample 12 (HPMC as a stabilizer), c) Sample 8 (PVA), d) Sample 2 (CHI) and e) Sample 14 (PEG).

(sample 4), CHI (sample 11) and PEG (sample 3)). On this figure, the experimental results and outcomes of modeling with different kinetic models are shown by scattered dots and solid lines, respectively. These models will be examined in more detail later. The obtained results confirm the promising potentials of the US-RESOLV technique to ameliorate in vitro dissolution rate and anticancer efficiency of the poorly soluble medicines, e.g. Sunitinib malate.

As shown in Fig. S1, the dissolution rate of the processed Sunitinib malate augmented (for example in Fig. S1(d), 72% of encapsulated drug was released in 15 min) corresponding to the its unprocessed form (39% in 15 min).

NPs of Sunitinib malate had a higher surface area than its original form in the solution. Enhanced solubility in water and dissolution rate of the processed Sunitinib malate by US-RESOLV might be explained by miniaturization and appropriate size distribution of the drug particles.

This could be linked to the ameliorated wetting features of the drug in a dissolution medium, larger specific surface area, and transformation from the crystalline to the amorphous phase (as per outputs shown by XRD and DSC analysis) [79]. Moreover, amorphous state has been more soluble because there is no need to energy for breaking up the crystal lattice in the course of the dissolution procedure. That is, a combined effect of the absence of a long-range molecular order as well as existence of the greater Gibbs free energy justifies faster dissolution rate with the amorphous drug particles [57,80]. In addition, initial release rate in four samples was relatively high. For example, for sample 4, cumulative percent release reached 66% within 15 min, while the rates decreased subsequently, so that the cumulative percent release reached 83% and 88% within 60 and 120 min, respectively. The higher dissolution rate in the initial stages could be associated with the medicine dissolution over the micro or nanoparticles' surface. Later on, drug
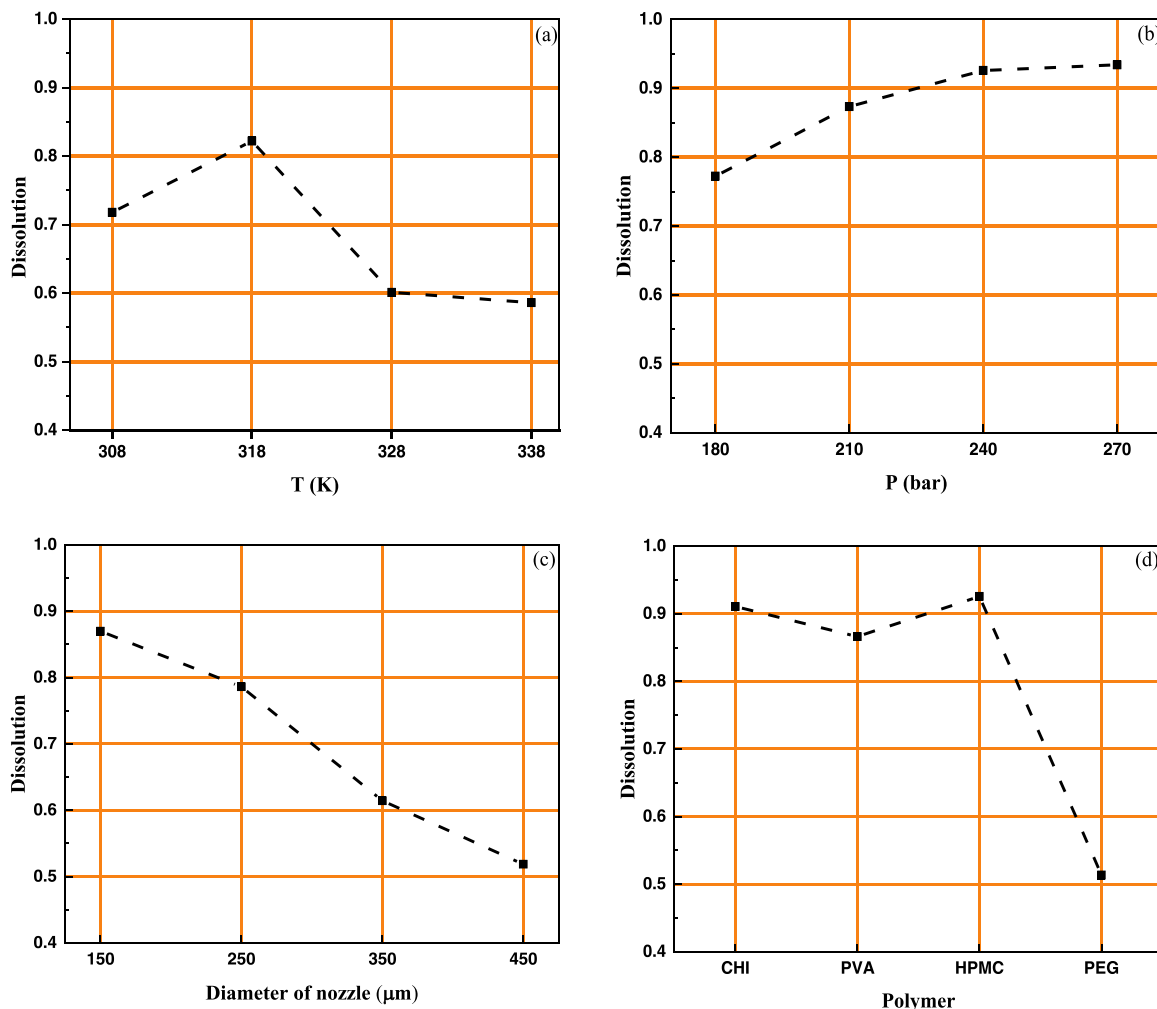
Fig. 4. The plot of US-RESOLV procedure for dissolution rate as a function of a) temperature, b) pressure, c) diameter of nozzle, and d) type of polymer.

release was mainly driven by a diffusion procedure that is a much slower mechanism.

A two-stage release profile of the Sunitinib malate from various samples demonstrated the diffusion-controlled dissolution of Sunitinib malate from all evaluated polymeric structures. Similar results have been published for Sunitinib malate from self-nanoemulsifying drug delivery systems in the literature [2].

Studying the kinetics of the drug release out of a polymer solution, one can not only describe the molecular patterns of dissolution of the active species, but also refine the stability of the drug. In this respect, the adjustable parameters provided by correlating different kinetics models to experimental data can analyze the release process [4,81]. In this research, mathematical models including Korsmeyer-Peppas, zero-order, Higuchi and Weibull have been utilized for correlating the experimental data.

Zero-order model, Eq. (2) illustrates releasing the drug from different drug delivery systems, as polymeric solution.

$$Q_t = Q_0 + K_0 t \tag{2}$$

where Q_t represents the amount of drug in time t, Q_0 refers to initial amounts of the drug in solution that is generally $Q_0 = 0.0$ M, and K_0 stands for the zero-order rate constant (concentration/time). Moreover, t represents time. In addition, zero order kinetic model considers concentration-independent release of the medicine at a constant rate [2,4].

Korsmeyer-Peppas [82] presented exponential relation, as follows:

$$\frac{Q_t}{Q_\infty} = K_p t^n \tag{3}$$

where $\frac{Q_t}{Q_\infty}$ represents fraction of the released drug by the time t and K_p refers to the constant that incorporates structural features of polymer and the drug and diffusional exponent, n, can be used to identify the process by which the drug is released out of the polymer. This relationship is applied to explain Fickian and nonFickian release behavior of the swelling-controlled release system. The release of the solute from the sheet, cylinder, sphere as well as the polydisperse specimens was analyzed. Diffusional exponent can provide valuable information on diffusional release mechanisms of a pharmaceutical compound from the polymeric system [2,83]

For Higuchi model:

$$Q_t = K_h t^{0.5} \tag{4}$$

here k_h represents Higuchi rate constant [81].

For Weibull model:

$$m = 1 - exp\left[\frac{-t^b}{a}\right] \tag{5}$$

so that m indicates time-variant fraction of Sunitinib malate dissolved in the simulated intestinal medium. As seen, it possesses 2 adjustment parameters of a and b that may have an optimal fitness to the dissolution data. The dissolution rate coefficient (K_w) is used to compare dissolution rates of the unprocessed and processed samples [17]. The K_w is calculated by the adjustment parameters of model, as follows:

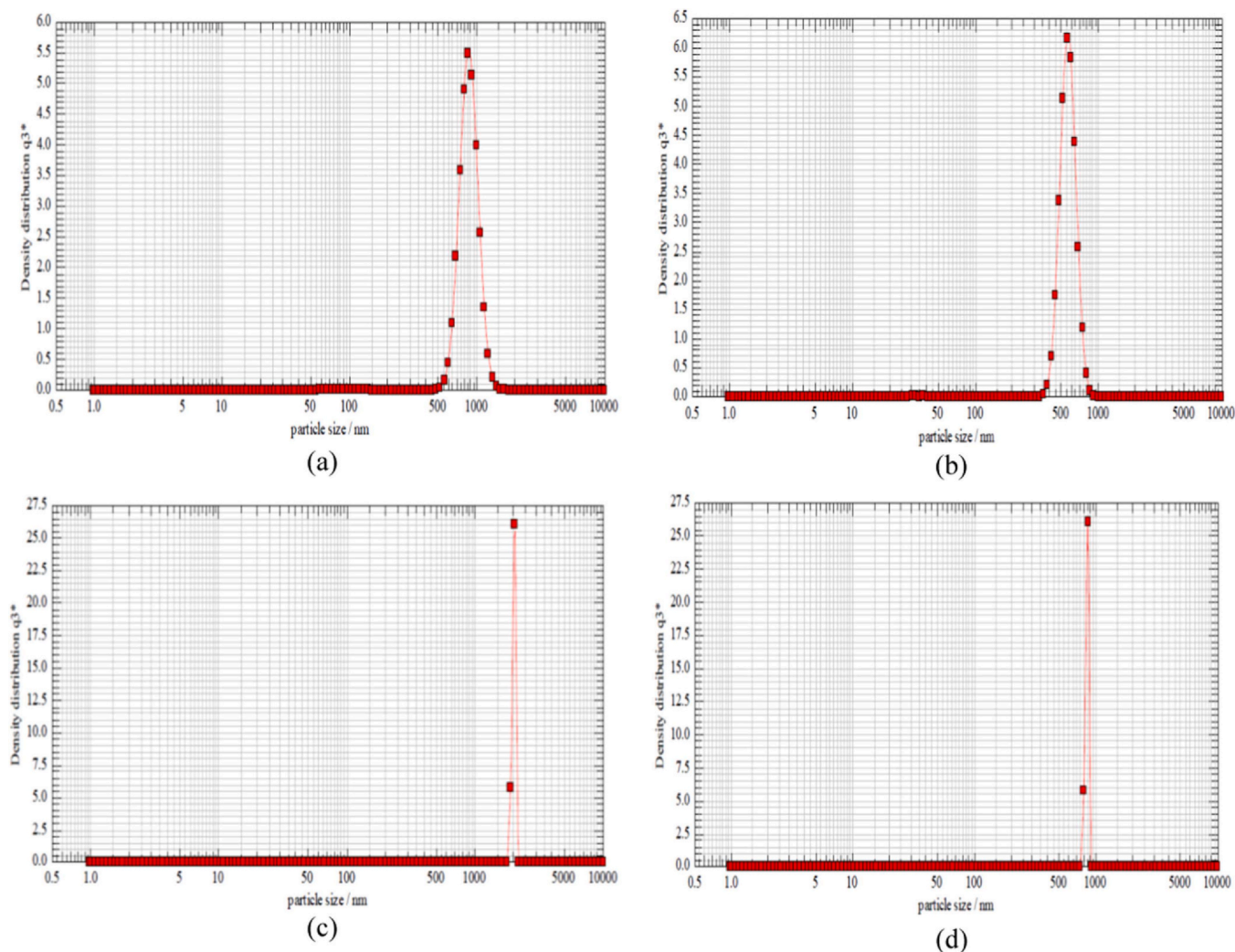$$K_w = \frac{1}{\sqrt[b]{a}} \tag{6}$$

Fig. 5. DLS graphs for a) Sample 1 b) Sample 10 c) Sample 2 and d) Sample 15.

According to Fig. S1, it can be concluded that Korsmeyer-Peppas and Weibull models had the best fit (high correlation coefficients R^2) to the experimental dissolution rate data. The correlation results including R^2, adjustable parameters and dissolution rate coefficient of samples of 5, 4, 11 and 3 and also original drug have been reported by Table S1. By reviewing Table S1, it could be stated R^2 values of Weibull model were slightly higher than those of Korsmeyer-Peppas model, which implied that the Weibull model was the most accurate mathematical model for investigated particles.

Examination of the diffusional exponent, n, for different samples showed that the samples prepared with using PVA, CHI and PEG, as the stabilizer, had n values smaller than or equal to 0.43, while those where HPMC was used as the stabilizer exhibited diffusional exponents beyond 0.43 but still lower than 0.85. There is enough information that in case of $n \leq 0.43$, Fickian diffusion of the drug would be observed through the polymer. Nonetheless, in case of $n > 0.43$ and < 0.85, the drug release mechanism would be a non-Fickian diffusion mechanism, where contributions from the medicine diffusion as well as polymer relaxation could be compared. If $n \geq 0.85$, we are facing a type-II diffusion process where the diffusion rate is considerably higher than the relaxation rate [4,83]. Therefore, it can be stated that the Sunitinib malate release from PVA, CHI and PEG polymers corresponded to the Fickian diffusion, while for HPMC-whose n value was 0.48-it followed non-Fickian diffusion mechanism and the polymer relaxation as well as drug diffusion participated in releasing Sunitinib malate. In addition, n value for original drug was 0.02, which this indicated that medicine has been released by Fickian diffusion mechanism.

With regard to Weibull model, the parameter K_w denotes the rate constant of the drug release [74]. As presented in Table S1, the obtained values of K_w for the processed Sunitinib malate by US-RESOLV method were higher than that for unprocessed Sunitinib malate because the drug diffused from the polymeric structures at the increased rates.

Taguchi experimental technique has been applied for examination of the impact of four operating variables used in NPs production on the dissolution rate of produced particles. The most basic step in the DoE is to properly select the factors (variables) and their levels. In this research, this basic stage was done on the ground of a review on the literature reporting the production of pharmaceutical NPs by using US-RESOLV approach [27,57]. The ANOVA was done by the experimental data presented in Table 2. Statistical evaluation of the outcomes provided us with the relative significance of different parameters affecting the response. The results in Table 4 revealed that the nozzle diameter (p = 0.0044) and type of polymer (p = 0.0024) used in the particle production using US-RESOLV are the most significant parameters that can influence on the dissolution rate. It should be noted that other parameters including temperature (p = 0.0127) and pressure (p = 0.0384) also have the significant effects on the dissolution rate. The 'Model F-value' of 41.59 (p = 0.0053) proved the significance of the model. However, just a 0.53% probability existed so that a large Model F-value occurred because of the noise. As a measure of comparison precision, CV was low enough (6.42%) to approve the accuracy and reliability of the experimental data. Moreover, corresponding value of R^2 to dissolution rate of the processed Sunitinib malate was 0.9940
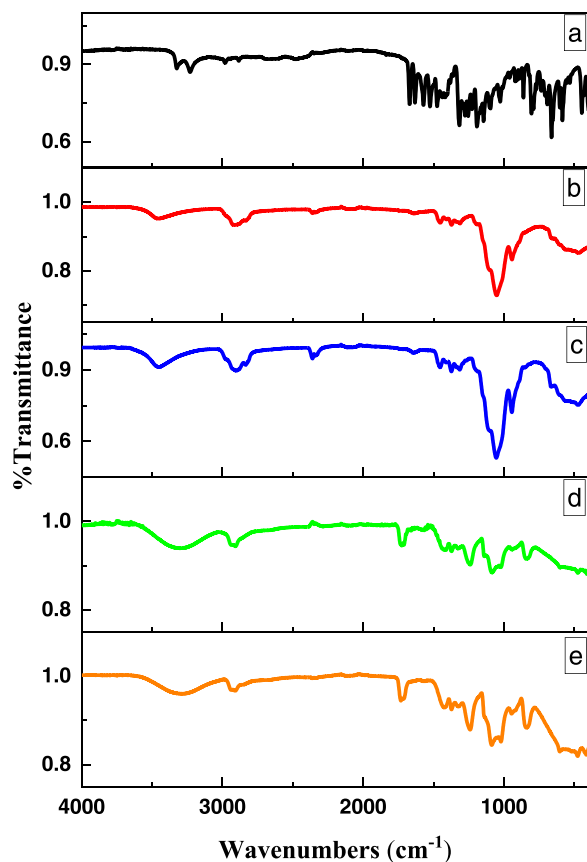
Fig. 6. Comparing FTIR spectrum of a) the original Sunitinib malate, b) HPMC, c) Sample 5, d) PVA and e) Sample 8.

Fig. 7. Comparing FTIR spectrum of a) original Sunitinib malate, b) CHI, c) Sample 2, d) PEG and e) Sample 14.

(Table 4); implying that the developed model was adequate for explaining 99.40% of the variance in responses. In addition, R^2_{pred} (0.8300) agreed reasonably with the adjusted R^2 (0.9701). As a measure of the ratio of signal to noise, the value of "Adeq. Precision" (20.42) significantly exceeded the generally desired baseline of 4 that is signal has been sufficiently without any noises. Furthermore, the predicted residual sum of squares; that is, the sum of squares of the difference between predicted as well as actual values over the entire set of experimental data points, PRESS = 0.17) prepares a measure of the goodness-of-fit of the model to the search points in the design. Consequently, if there is smaller PRESS, model would further fit with the data points [84]. Finally, results presented in this section prove that the Taguchi's DoE could well lead us toward the objectives of the present research.

Fig. 4a presents the influence of temperature on the dissolution rate (notably, at a temperature in which particles have been produced by the US-RESOLV method). It indicated that 318 K was the optimum temperature for production of NPs using the US-RESOLV method with the aim of having the highest dissolution rate. At the pressure of 240 bar, nozzle diameter of 450 μm and using HPMC polymer as stabilizer, increasing temperature from 308 to 318 K increased dissolution rate; while increasing the temperature between 318 and 328 K led to significant decline in dissolution rate. Also, rising temperature to 338 K caused a partial decline in dissolution rate of the drug.

According to Fig. 4b, the applied pressure for NPs production by US-RESOLV method and their dissolution rate are directly proportional. At 308 K, the nozzle with 250 μm diameter and by using PVA polymer, as the pressure increased, the dissolution rate increased. According to an earlier discussion, pressure imposed a significant effect on the increasing solubility and put differently, the rate of dissolution of pharmaceutical compounds would be concentration-dependent, meaning the increased amount of the released drug by enhancing drug concentration [81].
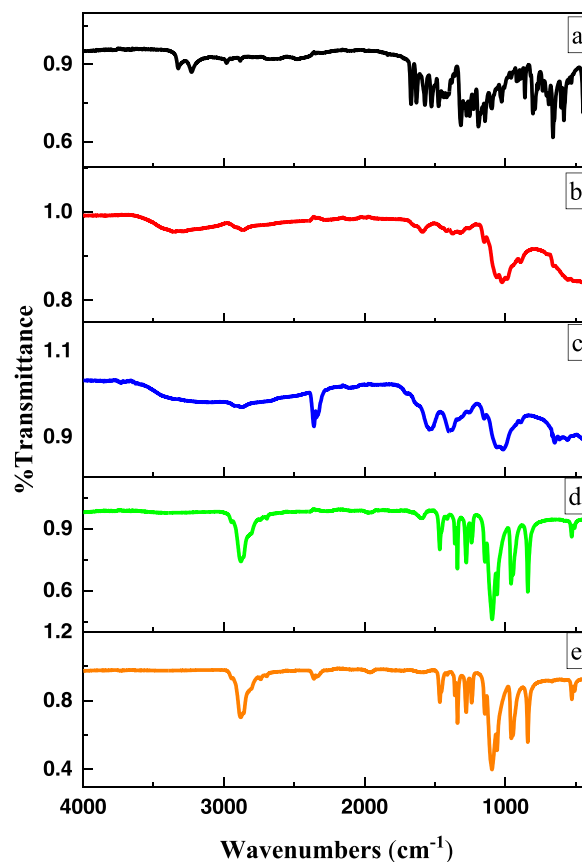
Another parameter that can affect dissolution rate of processed Sunitinib malate is the nozzle diameter used in the production of particles. Fig. 4c shows that at 338 K, the pressure equal to 210 bar by using CHI polymer, the smaller the diameter of the nozzle used in the US-RESOLV method, the higher the release rate of the particles produced. As a matter of fact, the fluid tended to exhibit a more linear velocity with reducing the nozzle diameter; this disturbed the balance between the nucleation and the particle growth and hence decreased the particle size.

In the following, four polymeric environments (HPMC, PVA, CHI and PEG) at a certain concentration (1% w/v) in the US-RESOLV method were utilized for investigating impact of stabilizer type on dissolution rate.

The rate at which the drug is released is known to be affected by the matrix structure and physicochemical features of polymer and drug. In meantime, however, medicine release profiles exhibit two characteristic stages, namely an early rapid release stage followed by a relatively constant-release rate stage dominated by the diffusion and degradation mechanisms [81,85].

Fig. 4d presents the relationships between dissolution rate and type of used polymer. According to Fig. 4d, it can be concluded that HPMC was the best polymer compared to other polymers for formation of particles with higher dissolution rate. Additionally, CHI dissolution rate has been higher than PVA. Moreover, PVA was higher than PEG.

The process of drug release begins by releasing drug from the NPs surface followed from the inner part of the NPs. The drug burst occurs by either releasing the adsorbed drug over the surface of polymer or leaching drug out of wider pores in the vicinity of the nanoparticle surface. The secondary stage is obviously related to the not only the polymer molecular weight, crystallinity and polarity, but also the drug load and particle size distribution as well as the matrix porosity. In this respect, one may expect a higher release rate with a highly porous
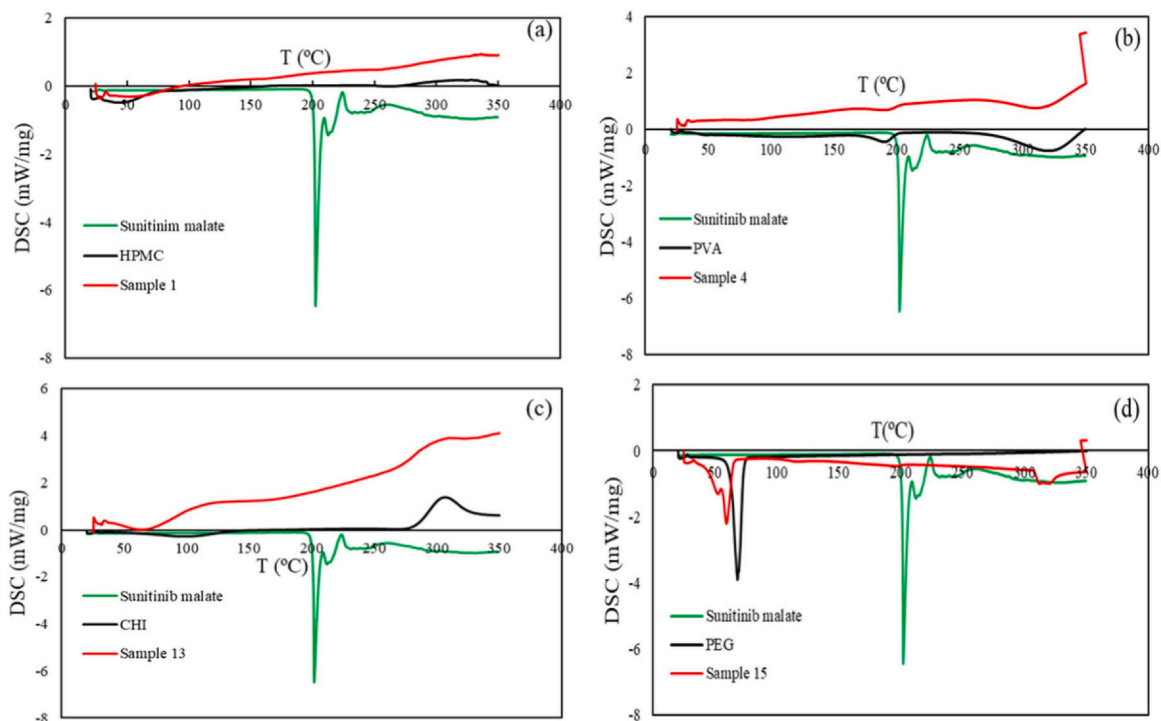
Fig. 8. DSC analysis results of a) Sample 1, b) Sample 4, c) Sample 13 and d) Sample 15, before and after process.
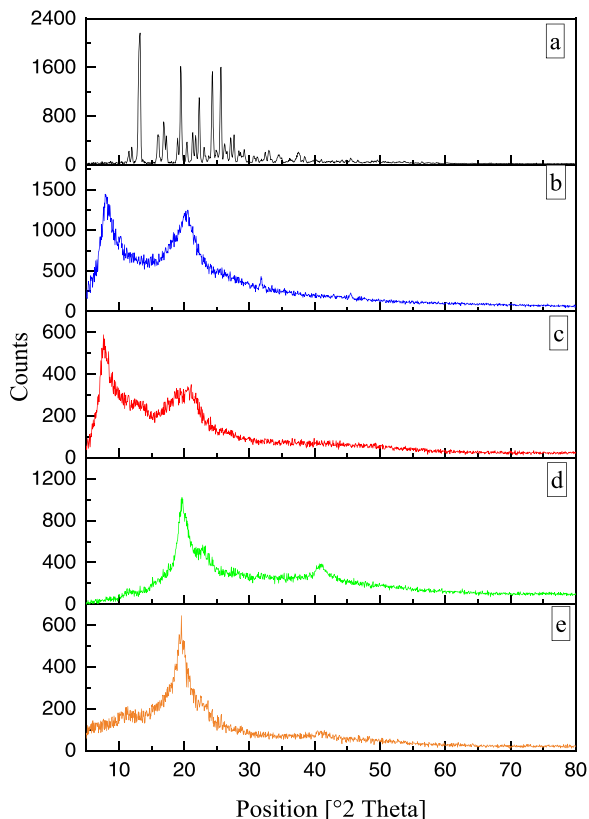

Fig. 9. XRD patterns of Sunitinib malate-polymer prior to and following the procedure a) the original Sunitinib malate, b) HPMC, c) Sample 1, d) PVA and e) Sample 4.
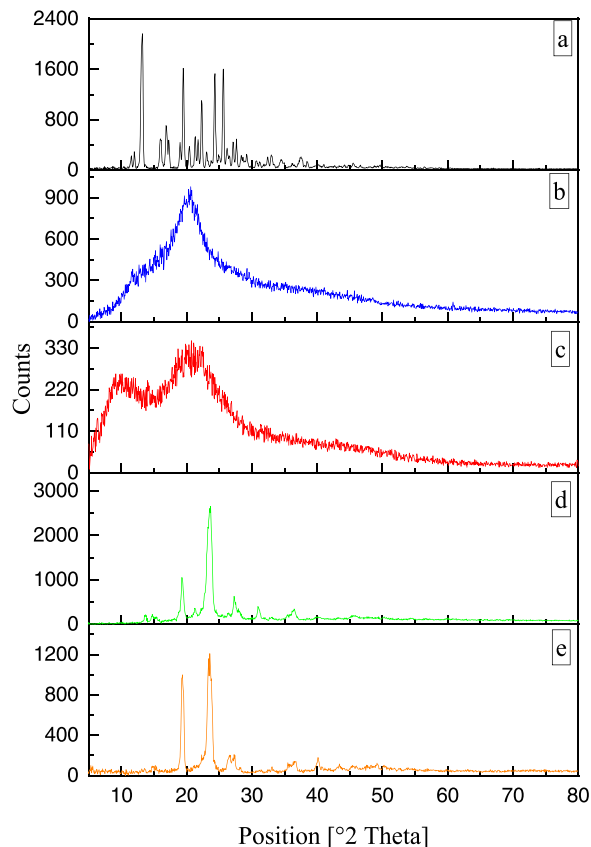
Fig. 10. XRD patterns of Sunitinib malate-polymer prior to and following the procedure a) original Sunitinib malate, b) CHI, c) Sample 13, d) PEG and e) Sample 14.

matrix. Total pore space in the polymeric structure has been seen to impose significant impacts on the release rate of medicine [85]. Generally, dissolution rate of medicine has been controlled by a different factors including the drug solubility and water absorption behaviors,

polymer swelling, and the drug-polymer interactions in terms of diffusion.

Compared to denser structures, porous structures exhibit less desirable mechanical characteristics in many applications. For a drug

delivery system, however, the porosity is crucial for not only the diffusion of pharmaceutical compounds and nutrients, but also cell migration and tissue growth [86]. Studies have shown that a larger pore size and/or further interconnectivity of the pores lead to a higher water uptake capacity for the respective scaffolds [87]. The swelling and penetrability of the polymer matrix have been identified to significantly influence drug dissolution rate. Therefore, as mentioned in previous section, HPMC has both high swelling characteristics and the irregular pores in large sizes inside itself, whereas, CHI, PVA and especially PEG have a wide pore size distribution with small pore sizes. Moreover, HPMC possesses a channeled micro-structure form in case of entering water into the polymer in the course of swelling process. The channels allowed the compacts for maintaining their forms during slow diffusion of drug between them. Such a fully homogeneous micro-structure would be established since HPMC swelling occurred slowly and the outer layers become the swollen but core remained un-swollen till the external gel eroded and water reached the core [74,88].

The SEM graph of CHI (Fig. 3d) indicates its sponge-like structure with numerous pores. This explains the dissolution performance of Sunitinib malate from CHI despite its average swelling capacity. This structure for CHI was observed in the previous research [74].

The effect of used polymer on the release rate can also be examined in terms of solubility parameter. Calculated as a square root of cohesive energy density, then, the solubility parameter provides a measure of polarity and ranges from about 14 (lowest polarity) to 48 MPa$^{1/2}$ (highest polarity). Despite the potentials of the parameter for the drug release studies, rare research works have actually used the δ in the pharmaceutics and biology fields [89]. There are several approaches to the evaluation of the solubility parameters, including direct measurements, correlation to one or more physical parameter, and indirect computations. For a polymer species, the so-called Hildebrand parameter (δ_t) cannot be obtained from the data on the vaporization heat, due to nonvolatility of the species. Accordingly, the only way to practically calculate the solubility parameters for a polymer is the indirect measurement. Among others, solubility parameters can be used for selecting compatible solvent for polymer and forecasting the swelling of the cured elastomers, the solvent vapor pressures in the polymer solution, and the polymer–polymer and multicomponent solvent phase equilibria. The relative equation for mixing enthalpy may be computed via Eq. (7):

$$\Delta h_m = \varphi_1 \varphi_2 (\delta_s - \delta_p)^2 \tag{7}$$

in which Δh_m indicates the per-unit-volume enthalpy of mixing, δ_p and δ_s denote the polymer and solvent solubility parameters, respectively. Eq. (7) sets that $\Delta h_m = 0$ provided $\delta_s = \delta_p$. That is, any 2 materials with the same solubility parameter must be reciprocally soluble because of their less-than-zero entropy factor. This supports the generally accepted law of improved solubility with similar chemical and structural properties. On the other hand, with increasing the gap between δ_s and δ_p, solute exhibits less tendency towards dissolving in the solvent [55]. In this research, the solubility parameter of the polymers has been computed via by using Fedors's technique [90]. The solubility parameter of HPMC, PVA, CHI and PEG was obtained 17.07, 16.60, 15.72 and 9.37 (cal cm^{-3})$^{0.5}$, respectively. The above values have consistency with the values presented in literature [56,89,91,92]. As mentioned before, the larger the solubility parameter, the more polar the polymer. In fact, when the difference between solubility parameter of water (23.40 (cal cm^{-3})$^{0.5}$) and polymer decreases and the tendency of polymer towards dissolution increases. Therefore, these outputs related to the impacts of type of used polymer on dissolution rate can be justified. It should be noted that PVA is a linear aliphatic hydrophilic polymer while chitosan has been considered as one of the cyclo-aliphatic hydrophilic polymers. Hence, the structure of PVA is usually regarded with higher compaction in comparison to chitosan [54]. Although PVA has a higher solubility parameter than CHI, but this structural difference results in PVA having a lower release rate than

chitosan. This structural difference was reported in the previous research [54]. Introduction of chitosan at small dosages could distort certain portions of the compact network of PVA, enlarging the pore space within the network. Therefore, higher dosages of chitosan in the membrane enhance its rate of permeation. This is while the permeation rate became lower with increasing the PVA dosage in the membrane, possibly due to the structural characteristics of the CHI and PVA [54].

DoE refers to the application of experimental designs to develop poly-nomial equation as well as the trace responses over an experimental domain for evaluation of optimal values of the considered parameters and the respective model [79]. Finally, the optimized condition for achieving the most acceptable rate of dissolution of Sunitinib malate have been defined as follows: 308 K, 270 bar pressure, 250 μm diameter of nozzle, using HPMC polymer as a stabilizer. Under the optimal set of conditions, the maximum dissolution rate (at 120 min) was found to be 0.9934.

3.3. Sunitinib malate characterization

FESEM analyses have been employed for characterizing morphology and structure of original Sunitinib malate and NPs produced by the US-RESOLV method. The results are presented in Fig. 3. Moreover, SEM images of original Sunitinib malate (Fig. 3a) indicates that the drug was composed of crystals with the irregular size and morphology. According to the comparison of the SEM pictures in Fig. 3, we found diminishment in the particle size using US-RESOLV method. Also, the images indicate entrapment of the drug NPs inside the carrier matrix and that carriers may suppress the crystal development of Sunitinib malate throughout this procedure. However, SEM outputs clarified the US-RESOLV method can reduce the particle size significantly and prepare NPs with homogeneous surface morphology; this showed complete dispersion of Sunitinib malate particles across the polymer.

The DLS curves in Fig. 5 indicate the homogeneous and uniform distribution of the drug in the used polymers. These curves were applied to calculate the SPAN values. The ultrasonication could interrupt the growth of the drug particles in the polymer in the course of the process. Indeed, the polymer could limit the NPs growth even with no strong interaction with the Sunitinib malate and by rather developing a corona encompassing the primary particles. Different methods have been used to enhance bioavailability of pharmaceutical compounds by improving their dissolution rate and solubility. Among all the methods, nanosizing techniques have received a lot of attention to enhance the rate of dissolution via extending specific surface areas of the poorly water soluble drug and hence adding to the respective oral bioavailability.

The polymer-drug molecular interactions were corroborated by FTIR spectra [53]. Figs. 6 and 7 indicate the IR spectra of pure Sunitinib malate, HPMC, sample 5, PVA, sample 8, CHI, sample 2, PEG and sample 14 in absorption bands in the ranges between 400 cm^{-1} and 4000 cm^{-1}. Fig. 6a shows that there are many sharp peaks in the fingerprint region of 400–1600 cm^{-1} for pure Sunitinib malate. Consequently, characteristic absorption band of C–F is situated at the 1026 cm^{-1} wavenumber. Moreover, the peaks have been seen at 1640 cm^{-1} for –NH–C=O, 2850 cm^{-1} associated with C–H (alkyl), 2960 cm^{-1} for the HC=CH (aryl), 3340 cm^{-1} specific to O–H (acid), N–H.

Therefore, acquired IR spectrum of HPMC is observed in Fig. 6b. This spectrum has been thoroughly investigated in the previous studies [93,94].

The FTIR spectrum of sample 5 is presented in Fig. 6c. This spectrum demonstrates all the characteristic peaks of HPMC during the US-RESOLV process and determines that Sunitinib malate was successfully entrapped by HPMC polymer. The noncovalent interaction like the hydrogen bonding that generally led to the typical peak shift or widening of the drug functional groups in the infrared spectroscopy tests [3]. Results of the sample 5 have been as the same as the HPMC spectrum. The obtained outputs did not show any considerable or

strong interactions between carrier and medicine. Nonetheless, because of lower content of drug in the solid dispersion, it is hard to detect it in FTIR tests or it is possible that typical bands of Sunitinib malate are masked by a polymer absorptive band in a similar location that consequently conceals any probable interaction like hydrogen-bonding [80,95].

For PVA (Fig. 6d), the intense band from $3550\,cm^{-1}$ to $3200\,cm^{-1}$ has been observed which is corresponded to OH from inter-molecular as well as intra-molecular hydrogen bonds. Moreover, spectrum has been examined in more detail in the previous researches [50,96,97]. On the other hand, spectrum of sample 8 (Fig. 6e) compared to the spectrum of PVA (Fig. 6d) shows that characteristic peaks of sample 8 were similar to the spectrum of PVA. This indicates that Sunitinib malate was successfully entrapped by PVA polymer.

FTIR spectrum of CHI is presented in Fig. 7b, where the corresponding peaks to CHI are observable at certain wavenumbers. Thus, the peak at $3356\,cm^{-1}$ was ascribed to $-NH_2$ and $-OH$ groups stretching vibrations. The amide I, II, and III vibrations were located at 1633, $1585\,cm^{-1}$ and $1318\,cm^{-1}$, respectively. Finally, peak at 1025 and $1070\,cm^{-1}$ indicated C–O stretching vibration [50,53,98,99].

FTIR spectrum of sample 2 can be seen in Fig. 7c. This proved that Sunitinib malate was well entrapped by CHI polymer. Additionally, peaks at $3356\,cm^{-1}$ for $-OH$ or $-NH_2$ groups was switched to $3310\,cm^{-1}$ with increasing the bandwidth, highlighting the formation of polymer-drug hydrogen bonds.

At the end, Fig. 7d and e shows FTIR spectra of PEG polymer and sample 14, respectively. The peak at 1094 as well as $1279\,cm^{-1}$ were attributed to O–H and C–O–H stretching. Moreover, the peaks at 1341 and $1466\,cm^{-1}$ indicated C–H bending. In addition, the peaks that were situated in 2878 and $3423\,cm^{-1}$ were caused by C–H as well as O–H stretching in PEG polymer, respectively [100]. The results of the sample 14 were similar to the spectrum of PEG. This proved that Sunitinib malate was well entrapped by PEG polymer.

Fig. 8 presents the outcomes of the DSC analysis on pure Sunitinib malate, pure polymers, sample 1, sample 4, sample 13, and sample 15. Pure Sunitinib malate showed 208 °C melting point (T_m) (as per the respective characteristic endothermic peak), showing that the original Sunitinib malate was in the crystalline phase. This was in good agreement with a previous finding [3]. The DSC analysis of the pure HPMC (Fig. 8a) showed that the endothermic transition occurred in ranges from 35 to 75 °C and a wide peak exhibited in the midway, well approving the findings of a previous research work [101]. Fig. 8b shows a characteristic peak for PVA at about 190 °C, this value is consistent with other researches [102].

The DSC curve of CHI (Fig. 8c) indicated one endothermic and one exothermic peak in the ranges of 94–105 °C and 306–308 °C, respectively. Also known as dehydration temperature (T_D), the endothermic peak signified the water removal from the hydrophilic groups on the chitosan. As a polysaccharide, chitosan exhibits a disordered structure in the solid state, in which condition it exhibits high affinity toward hydration. The endothermic peak highlighted that the chitosan was yet to be fully dehydrated, with some bound water remained even after the drying stage. The exothermic peak, on the other hand, characterized chitosan thermal degradation of (glycoside bond cleavage, decomposition of de-acetylated and acetyl units, and monomer dehydration) [103].

As shown by the DSC curve of PEG (Fig. 8d), the melting point has been observed at 67 °C. This value is consistent with other researches [104]. According to the DSC results of considered samples (1, 4, 13 and 15) in Fig. 8, it can be concluded that the endothermal peak of drug was disappeared which confirmed complete entrapment of drug into polymers matrix and so the degree of crystallinity of drug was decreased.

The crystallinity of the Sunitinib malate was further analyzed by means of the XRD analysis (Fig. 9a). Based on the results (i.e. diffraction patterns), the original Sunitinib malate was found to be well crystalline with obvious peaks at diffraction angles (2θ) of 13.16°, 16.0°, 16.89°, 19.48°, 22.30°, 24.30° and 25.60°.

As presented in Figs. 9 and 10, XRD analysis of US-RESOLV indicated lower crystallinity of the processed drug compared to the original particles, probably due to their reduced particle size. The XRD patterns recorded from the particles produced by US-RESOLV process exhibited no characteristic peaks corresponding to Sunitinib malate; this was while broad peaks were observed, that indicated amorphous nature of the samples, just like those observed for the HPMC, PVA, CHI and PEG. Our findings well agreed with outputs obtained by DSC analyses, proving effectiveness of the US-RESOLV method for making the Sunitinib malate in the amorphous state.

4. Conclusion

The dissolution rate of the drug may be enhanced via miniaturizing size of the particles, especially to a nanometer scale, which this is able to significantly extend the specific surface area of the particles of drug and leads to considerably ameliorated bioavailability of drug. This research, for the first time, utilized US-RESOLV (Rapid Expansion of a Supercritical CO_2 Solution into a Liquid Solvent) method for controlling the size as well as size distribution of Sunitinib malate as a water- insoluble drug. In this method, the drug molecules may be enclosed by a polymeric shell or it may be smoothly distributed into it. In addition, mean size, morphology, and distribution of the pore sizes, molecular weight as well as polarity of polymers could affect dissolution rate and size distribution of drug particles. Choosing the proper polymer for dispersion of pharmaceutical compounds is considered as a challenge. In this regard, four polymeric stabilizers (HPMC, PVA, CHI and PEG) were selected to investigate their effects on the resultant particles size distribution (SPAN value) and dissolution rate. Also, the influences of pressure, nozzle diameter and temperature on the morphology, size distribution and dissolution rate of the produced particles have been studied and optimized using the Taguchi design procedure. Then, these particles have been investigated by a variety of physical characterization methods including FESEM, DLS, DSC, XRD, and FTIR analyses. In order to accomplish the research objectives, PEG was the best polymer for controlling the particle size distribution and HPMC served as the best polymeric stabilizer for increasing the dissolution rate of the Sunitinib malate particles. Sunitinib malate particles of 858.32, 560.93, 1017.85 and 843.26 nm in average diameter were fabricated via the US-RESOLV method by using HPMC, PVA, CHI and PEG, respectively. Kinetics model has been utilized to explain release mechanism of pharmaceutical substances from polymeric matrices. In this research, mathematical models including zero order, Korsmeyer-Peppas, Higuchi as well as Weibull have been utilized to correlate experimental dissolution rate. According to the outputs, Weibull model can correlate the experimental data with the highest accuracy. Miniaturization of the size of the particles as well as the presence of the hydrophilic polymers enhanced dissolution rate of the Sunitinib malate in the aqueous solutions significantly. To sum up, it was concluded that, when devised with appropriate polymer stabilizer and ultrasonication, the US-RESOLV method can effectively inhibit the particle agglomeration and rather accelerate the dissolution and control the distribution of the particles' size of the Sunitinib malate as a weakly soluble drug in aqueous medium.

Declaration of Competing Interest

The authors declare that they have no known competing financial interests or personal relationships that could have appeared to influence the work reported in this paper.

Acknowledgement

Appendix A. Supporting information

Supplementary data associated with this article can be found in the online version at doi:10.1016/j.supflu.2021.105163.

References

[1] S. Sangwan, T. Panda, R. Thiamattam, S.K. Dewan, R.K. Thaper, Novel salts of Sunitinib an anticancer drug with improved solubility, Int. Res. J. Pure Appl. Chem. 5 (2015) 352–365.

[2] S.M. Alshahrani, A.S. Alshetaili, A. Alalaiwe, B.B. Alsulays, M.K. Anwer, R. Al-Shdefat, F. Imam, F. Shakeel, Anticancer efficacy of self-nanoemulsifying drug delivery system of Sunitinib malate, AAPS PharmSciTech 19 (2018) 123–133.

[3] A.S. Alshetaili, M.K. Anwer, S.M. Alshahrani, A. Alalaiwe, B.B. Alsulays, M.J. Ansari, F. Imam, S. Alshehri, Characteristics and anticancer properties of Sunitinib malate-loaded poly-lactic-co-glycolic acid nanoparticles against human colon cancer HT-29 cells lines, Trop. J. Pharm. Res. 17 (2018) 1263–1269.

[4] O.I. Parisi, C. Morelli, L. Scrivano, M.S. Sinicropi, M.G. Cesario, S. Candamano, F. Puoci, D. Sisci, Controlled release of Sunitinib in targeted cancer therapy: smart magnetically responsive hydrogels as restricted access materials, RSC Adv. 5 (2015) 65308–65315.

[5] H.G. Brittain, Profiles of Drug Substances, Excipients, and Related Methodology, Academic press, 2013.

[6] E. Weidner, High pressure micronization for food applications, J. Supercrit. Fluids 47 (2009) 556–565.

[7] G. Sodeifian, F. Razmimanesh, S.A. Sajadian, Solubility measurement of a chemotherapeutic agent (Imatinib mesylate) in supercritical carbon dioxide: assessment of new empirical model, J. Supercrit. Fluids 146 (2019) 89–99.

[8] G. Sodeifian, F. Razmimanesh, N.S. Ardestani, S.A. Sajadian, Experimental data and thermodynamic modeling of solubility of Azathioprine, as an immunosuppressive and anti-cancer drug, in supercritical carbon dioxide, J. Mol. Liq. 299 (2020) 112179.

[9] G. Sodeifian, N.S. Ardestani, F. Razmimanesh, S.A. Sajadian, Experimental and thermodynamic analyses of supercritical CO2-solubility of minoxidil as an antihypertensive drug, Fluid Phase Equilib. 522 (2020) 112745.

[10] D. Liu, H. Pan, F. He, X. Wang, J. Li, X. Yang, W. Pan, Effect of particle size on oral absorption of carvedilol nanosuspensions: in vitro and in vivo evaluation, Int. J. Nanomed. 10 (2015) 6425.

[11] M.J. Cocero, Á. Martín, F. Mattea, S. Varona, Encapsulation and co-precipitation processes with supercritical fluids: fundamentals and applications, J. Supercrit. Fluids 47 (2009) 546–555.

[12] N. Esfandiari, Production of micro and nano particles of pharmaceutical by supercritical carbon dioxide, J. Supercrit. Fluids 100 (2015) 129–141.

[13] P. Gosselin, R. Thibert, M. Preda, J. McMullen, Polymorphic properties of micronized carbamazepine produced by RESS, Int. J. Pharm. 252 (2003) 225–233.

[14] P.-C. Lin, C.-S. Su, M. Tang, Y.-P. Chen, Micronization of tolbutamide using rapid expansion of supercritical solution with solid co-solvent (RESS-SC) process, Res. Chem. Intermed. 37 (2011) 153–163.

[15] E. Reverchon, R. Adami, Nanomaterials and supercritical fluids, J. Supercrit. Fluids 37 (2006) 1–22.

[16] E. Reverchon, R. Adami, S. Cardea, G. Della Porta, Supercritical fluids processing of polymers for pharmaceutical and medical applications, J. Supercrit. Fluids 47 (2009) 484–492.

[17] G. Sodeifian, S.A. Sajadian, Solubility measurement and preparation of nanoparticles of an anticancer drug (Letrozole) using rapid expansion of supercritical solutions with solid cosolvent (RESS-SC), J. Supercrit. Fluids 133 (2018) 239–252.

[18] T. Kodama, M. Honda, R. Takemura, T. Fukaya, C. Uemori, H. Kanda, M. Goto, Effect of the Z-isomer content on nanoparticle production of lycopene using solution-enhanced dispersion by supercritical fluids (SEDS), J. Supercrit. Fluids 133 (2018) 291–296.

[19] K. Kaga, M. Honda, T. Adachi, M. Honjo, H. Kanda, M. Goto, Nanoparticle formation of PVP/astaxanthin inclusion complex by solution-enhanced dispersion by supercritical fluids (SEDS): effect of PVP and astaxanthin Z-isomer content, J. Supercrit. Fluids 136 (2018) 44–51.

[20] Y. Bayat, S.M. Pourmortazavi, H. Ahadi, H. Iravani, Taguchi robust design to optimize supercritical carbon dioxide anti-solvent process for preparation of 2, 4, 6, 8, 10, 12-hexanitro-2, 4, 6, 8, 10, 12-hexaazaisowurtzitane nanoparticles, Chem. Eng. J. 230 (2013) 432–438.

[21] G. Sodeifian, F. Razmimanesh, S.A. Sajadian, H.S. Panah, Solubility measurement of an antihistamine drug (loratadine) in supercritical carbon dioxide: Assessment of qCPA and PCP-SAFT equations of state, Fluid Phase Equilib. 472 (2018) 147–159.

[22] G. Sodeifian, S.M. Hazaveie, S.A. Sajadian, F. Razmimanesh, Experimental investigation and modeling of the solubility of oxcarbazepine (an anticonvulsant agent) in supercritical carbon dioxide, Fluid Phase Equilib. 493 (2019) 160–173.

[23] N.S. Ardestani, G. Sodeifian, S.A. Sajadian, Preparation of phthalocyanine green nano pigment using supercritical CO2 gas antisolvent (GAS): experimental and modeling, Heliyon 6 (2020) e04947.

[24] G. Sodeifian, F. Razmimanesh, S.A. Sajadian, S.M. Hazaveie, Experimental data and thermodynamic modeling of solubility of Sorafenib tosylate, as an anti-cancer drug, in supercritical carbon dioxide: evaluation of Wong-Sandler mixing rule, J. Chem. Thermodyn. 142 (2020) 105998.

[25] S. Ghoreishi, A. Hedayati, M. Kordnejad, Micronization of chitosan via rapid expansion of supercritical solution, J. Supercrit. Fluids 111 (2016) 162–170.

[26] S. Ghoreishi, S. Komeili, Modeling of fluorinated tetraphenylporphyrin nanoparticles size design via rapid expansion of supercritical solution, J. Supercrit. Fluids 50 (2009) 183–192.

[27] G. Sodeifian, S.A. Sajadian, N.S. Ardestani, F. Razmimanesh, Production of Loratadine drug nanoparticles using ultrasonic-assisted Rapid expansion of supercritical solution into aqueous solution (US-RESSAS), J. Supercrit. Fluids 147 (2019) 241–253.

[28] N. Esfandiari, S.M. Ghoreishi, Kinetic modeling of the gas antisolvent process for synthesis of 5–fluorouracil nanoparticles, Chem. Eng. Technol. 37 (2014) 73–80.

[29] I. Akbari, S. Ghoreishi, N. Habibi, Generation and precipitation of paclitaxel nanoparticles in basil seed mucilage via combination of supercritical gas antisolvent and phase inversion techniques, J. Supercrit. Fluids 94 (2014) 182–188.

[30] A.Z. Hezave, F. Esmaeilzadeh, Micronization of drug particles via RESS process, J. Supercrit. Fluids 52 (2010) 84–98.

[31] M.J. Meziani, P. Pathak, W. Wang, T. Desai, A. Patil, Y.-P. Sun, Polymeric nanofibers from rapid expansion of supercritical solution, Ind. Eng. Chem. Res. 44 (2005) 4594–4598.

[32] M.J. Meziani, Y.-P. Sun, Protein-conjugated nanoparticles from rapid expansion of supercritical fluid solution into aqueous solution, J. Am. Chem. Soc. 125 (2003) 8015–8018.

[33] P. Pathak, M.J. Meziani, T. Desai, Y.-P. Sun, Nanosizing drug particles in supercritical fluid processing, J. Am. Chem. Soc. 126 (2004) 10842–10843.

[34] Y.-P. Sun, Supercritical Fluid Technology in Materials Science and Engineering: Syntheses: Properties, and Applications, CRC Press, 2002.

[35] I. Pasquali, R. Bettini, Are pharmaceutics really going supercritical? Int. J. Pharm. 364 (2008) 176–187.

[36] M.J. Meziani, P. Pathak, R. Hurezeanu, M.C. Thies, R.M. Enick, Y.P. Sun, Supercritical-fluid processing technique for nanoscale polymer particles, Angew. Chem. Int. Ed. 43 (2004) 704–707.

[37] P. Pathak, M.J. Meziani, T. Desai, Y.-P. Sun, Formation and stabilization of ibuprofen nanoparticles in supercritical fluid processing, J. Supercrit. Fluids 37 (2006) 279–286.

[38] A. Sane, M.C. Thies, The formation of fluorinated tetraphenylporphyrin nanoparticles via rapid expansion processes: RESS vs RESOLV, J. Phys. Chem. B 109 (2005) 19688–19695.

[39] M. Türk, Manufacture of submicron drug particles with enhanced dissolution behaviour by rapid expansion processes, J. Supercrit. Fluids 47 (2009) 537–545.

[40] M. Türk, D. Bolten, Formation of submicron poorly water-soluble drugs by rapid expansion of supercritical solution (RESS): results for naproxen, J. Supercrit. Fluids 55 (2010) 778–785.

[41] P. Pathak, G.L. Prasad, M.J. Meziani, A.A. Joudeh, Y.-P. Sun, Nanosized paclitaxel particles from supercritical carbon dioxide processing and their biological evaluation, Langmuir 23 (2007) 2674–2679.

[42] Y.-P. Sun, J.E. Riggs, H.W. Rollins, R. Guduru, Strong optical limiting of silver-containing nanocrystalline particles in stable suspensions, J. Phys. Chem. B 103 (1999) 77–82.

[43] Y.-P. Sun, R. Guduru, F. Lin, T. Whiteside, Preparation of nanoscale semiconductors through the rapid expansion of supercritical solution (RESS) into liquid solution, Ind. Eng. Chem. Res. 39 (2000) 4663–4669.

[44] M.J. Meziani, P. Pathak, L.F. Allard, Y.-P. Sun, Nanoparticle Formation in Rapid Expansion of Water-in-carbon Dioxide Microemulsion into Liquid Solvent, ACS Publications, 2003.

[45] P. Pathak, M.J. Meziani, Y.-P. Sun, Supercritical fluid technology for enhanced drug delivery, Expert Opin. Drug Deliv. 2 (2005) 747–761.

[46] V. Prosapio, Micronization by supercritical antisolvent precipitation processes, 2016.

[47] J. Djuris, S. Milovanovic, D. Medarevic, V. Dobricic, S. Dapčević, S. Ibric, Selection of the suitable polymer for supercritical fluid assisted preparation of carvedilol solid dispersions, Int. J. Pharm. 554 (2019) 190–200.

[48] Y. Huang, W.-G. Dai, Fundamental aspects of solid dispersion technology for poorly soluble drugs, Acta Pharm. Sin. B 4 (2014) 18–25.

[49] K. Deshmukh, M.B. Ahamed, R. Deshmukh, S.K. Pasha, P. Bhagat, K. Chidambaram, Biopolymer composites with high dielectric performance: interface engineering, in: K.K. Sadasivuni, D. Ponnamma, J. Kim, J.-J. Cabibihan, M.A. AlMaadeed (Eds.), Biopolymer Composites in Electronics, Elsevier, 2017, pp. 27–128.

[50] A. Bernal-Ballen, J.-A. Lopez-Garcia, K. Ozaltin, (PVA/Chitosan/Fucoidan)-Ampicillin: a bioartificial polymeric material with combined properties in cell regeneration and potential antibacterial features, Polymers 11 (2019) 1325.

[51] D. Chattopadhyay, M.S. Inamdar, Aqueous behaviour of chitosan, Int. J. Polym. Sci. 2010 (2010) 1–7.

[52] V.T. de Fávere, W.L. Hinze, Evaluation of the potential of chitosan hydrogels to extract polar organic species from nonpolar organic solvents: application to the extraction of aminopyridines from hexane, J. Colloid Interface Sci. 330 (2009) 38–44.

[53] B. Cai, T. Zhong, P. Chen, J. Fu, Y. Jin, Y. Liu, R. Huang, L. Tan, Preparation, characterization and in vitro release study of drug-loaded sodium carboxy-methylcellulose/chitosan composite sponge, PLOS ONE 13 (2018) e0206275.

[54] S.P. Campana-Filho, L.A. de Almeida Pinto, Chitosan Based Materials and its Applications, Bentham Science Publishers, 2017.

[55] C. Özdemir, A. Güner, Solubility profiles of poly (ethylene glycol)/solvent systems, I: qualitative comparison of solubility parameter approaches, Eur. Polym. J. 43 (2007) 3068–3093.

[56] J.M. Harris, Poly (ethylene glycol) Chemistry: Biotechnical and Biomedical Applications, Springer Science & Business Media, 2013.

[57] G. Sodeifian, S.A. Sajadian, Utilization of ultrasonic-assisted RESOLV (US-RESOLV) with polymeric stabilizers for production of amiodarone hydrochloride

nanoparticles: optimization of the process parameters, Chem. Eng. Res. Des. 142 (2019) 268–284.

[58] P.A. Mello, J.S. Pereira, M.F. Mesko, J.S. Barin, E.M. Flores, Sample preparation methods for subsequent determination of metals and non-metals in crude oil—a review, Anal. Chim. Acta 746 (2012) 15–36.

[59] K. Yasui, Acoustic Cavitation and Bubble Dynamics, Springer, 2018.

[60] F. Ali, L. Reinert, J.-M. Lévêque, L. Duclaux, F. Muller, S. Saeed, S.S. Shah, Effect of sonication conditions: solvent, time, temperature and reactor type on the preparation of micron sized vermiculite particles, Ultrason. Sonochem. 21 (2014) 1002–1009.

[61] M.Y. Masoomi, A. Morsali, P.C. Junk, J. Wang, Ultrasonic assisted synthesis of two new coordination polymers and their applications as precursors for preparation of nano-materials, Ultrason. Sonochem. 34 (2017) 984–992.

[62] P. Pathak, M.J. Meziani, T. Desai, C. Foster, J.A. Diaz, Y.-P. Sun, Supercritical fluid processing of drug nanoparticles in stable suspension, J. Nanosci. Nanotechnol. 7 (2007) 2542–2545.

[63] M.J. Meziani, H.W. Rollins, L.F. Allard, Y.-P. Sun, Protein-protected nanoparticles from rapid expansion of supercritical solution into aqueous solution, J. Phys. Chem. B 106 (2002) 11178–11182.

[64] S.-T. Xiang, B.-Q. Chen, R.K. Kankala, S.-B. Wang, A.-Z. Chen, Solubility measurement and RESOLV-assisted nanonization of gambogic acid in supercritical carbon dioxide for cancer therapy, J. Supercrit. Fluids 150 (2019) 147–155.

[65] P.-C. Lin, C.-S. Su, M. Tang, Y.-P. Chen, Micronization of ethosuximide using the rapid expansion of supercritical solution (RESS) process, J. Supercrit. Fluids 72 (2012) 84–89.

[66] A. Fattahi, J. Karimi-Sabet, A. Keshavarz, A. Golzary, M. Rafiee-Tehrani, F.A. Dorkoosh, Preparation and characterization of simvastatin nanoparticles using rapid expansion of supercritical solution (RESS) with trifluoromethane, J. Supercrit. Fluids 107 (2016) 469–478.

[67] G. Sodeifian, F. Razmimanesh, S.A. Sajadian, Prediction of solubility of sunitinib malate (an anti-cancer drug) in supercritical carbon dioxide (SC–CO2): experimental correlations and thermodynamic modeling, J. Mol. Liq. 297 (2020) 111740.

[68] I. Gouaou, S. Shamaei, M.S. Koutchoukali, M. Bouhelassa, E. Tsotsas, A. Kharaghani, Impact of operating conditions on a single droplet and spray drying of hydroxypropylated pea starch: Process performance and final powder properties, Asia-Pac. J. Chem. Eng. 14 (2019) e2268.

[69] J. Guan, P. Cheng, S.J. Huang, Z.H. Li, X.Z. Zhang, J.M. Wu, Y. Guo, R.X. Li, Study on preparation of chitosan microspheres loaded with levofloxacin, in: Fei Tang (Ed.), Key Engineering Materials, Trans Tech Publ, 2014, pp. 442–448.

[70] A. Rafie Tabar, N. Anarjan, S. Ghanbarzadeh, H. Hamishehkar, Effect of processing parameters on physicochemical properties of β-carotene nanocrystal: a statistical experimental design analysis, Iran. J. Pharm. Sci. 12 (2016) 77–92.

[71] P. Dayal, M.S. Shaik, M. Singh, Evaluation of different parameters that affect droplet-size distribution from nasal sprays using the Malvern Spraytec®, J. Pharm. Sci. 93 (2004) 1725–1742.

[72] A. Shahbazian, A. Davood, A. Dabirsiaghi, Application of Taguchi method to investigate the effects of process factors on the production of industrial Piroxicam polymorphs and optimization of dissolution rate of powder, Iran. J. Pharm. Res. 15 (2016) 395.

[73] J. Elversson, A. Millqvist-Fureby, G. Alderborn, U. Elofsson, Droplet and particle size relationship and shell thickness of inhalable lactose particles during spray drying, J. Pharm. Sci. 92 (2003) 900–910.

[74] F. Notario-Pérez, A. Martín-Illana, R. Cazorla-Luna, R. Ruiz-Caro, L.-M. Bedoya, A. Tamayo, J. Rubio, M.-D. Veiga, Influence of chitosan swelling behaviour on controlled release of tenofovir from mucoadhesive vaginal systems for prevention of sexual transmission of HIV, Mar. Drugs 15 (2017) 50.

[75] M.G. Cascone, L. Lazzeri, E. Sparvoli, M. Scatena, L.P. Serino, S. Danti, Morphological evaluation of bioartificial hydrogels as potential tissue engineering scaffolds, J. Mater. Sci. Mater. Med 15 (2004) 1309–1313.

[76] N. Kaneniwa, N. Watari, Dissolution of slightly soluble drugs. I. Influence of particle size on dissolution behavior, Chem. Pharm. Bull. 22 (1974) 1699–1705.

[77] A. Tromelin, S. Habillon, C. Andres, Y. Pourcelot, B. Chaillot, Relationship between particle size and dissolution rate of bulk powders and sieving characterized fractions of two qualities of orthoboric acid, Drug Dev. Ind. Pharm. 22 (1996) 977–986.

[78] J.øc Thur, M.N. Musa, Dissolution rate patterns of log-normally distributed powders, J. Pharm. Sci. 61 (1972) 223–227.

[79] V.M. Pandya, J.K. Patel, D.J. Patel, Formulation and optimization of nanosuspensions for enhancing simvastatin dissolution using central composite design, Dissolut. Technol. 18 (2011) 40–45.

[80] F. Frizon, J. de Oliveira Eloy, C.M. Donaduzzi, M.L. Mitsui, J.M. Marchetti, Dissolution rate enhancement of loratadine in polyvinylpyrrolidone K-30 solid dispersions by solvent methods, Powder Technol. 235 (2013) 532–539.

[81] D. Wójcik-Pastuszka, J. Krzak, B. Macikowski, R. Berkowski, B. Osiński, W. Musiał, Evaluation of the release kinetics of a pharmacologically active substance from model intra-articular implants replacing the cruciate ligaments of the knee, Materials 12 (2019) 1202.

[82] R.W. Korsmeyer, R. Gurny, E. Doelker, P. Buri, N.A. Peppas, Mechanisms of solute release from porous hydrophilic polymers, Int. J. Pharm. 15 (1983) 25–35.

[83] P.L. Ritger, N.A. Peppas, A simple equation for description of solute release II. Fickian and anomalous release from swellable devices, J. Control Release 5 (1987) 37–42.

[84] G. Sodeifian, S.A. Sajadian, Investigation of essential oil extraction and antioxidant activity of Echinophora platyloba DC. using supercritical carbon dioxide, J. Supercrit. Fluids 121 (2017) 52–62.

[85] O. Petrov, I. Furó, M. Schuleit, R. Domanig, M. Plunkett, J. Daicic, Pore size distributions of biodegradable polymer microparticles in aqueous environments measured by NMR cryoporometry, Int. J. Pharm. 309 (2006) 157–162.

[86] J. Boateng, Therapeutic Dressings and Wound Healing Applications, Wiley Online Library, 2020.

[87] M. Vahidi, M. Frounchi, S. Dadbin, Porous gelatin/poly (ethylene glycol) scaffolds for skin cells, Soft Mater. 15 (2017) 95–102.

[88] P. Hiremath, K. Nuguru, V. Agrahari, Material attributes and their impact on wet granulation process performance, in: Ajit S. Narang, Sherif I.F. Badawy (Eds.), Handbook of Pharmaceutical Wet Granulation, Elsevier, 2019, pp. 263–315.

[89] P. Bustamante, J. Navarro-Lupión, M. Peña, B. Escalera, Hildebrand solubility parameter to predict drug release from hydroxypropyl methylcellulose gels, Int. J. Pharm. 414 (2011) 125–130.

[90] R.F. Fedors, A method for estimating both the solubility parameters and molar volumes of liquids, Polym. Eng. Sci. 14 (1974) 147–154.

[91] R. Ravindra, K.R. Krovvidi, A. Khan, Solubility parameter of chitin and chitosan, Carbohydr. Polym. 36 (1998) 121–127.

[92] W. Zeng, Y. Du, Y. Xue, H. Frisch, Solubility parameters, in: James E. Mark (Ed.), Physical Properties of Polymers Handbook, Springer, 2007, pp. 289–303.

[93] G.R. Mahdavinia, S. Ettehadi, M. Amini, M. Sabzi, Synthesis and characterization of hydroxypropyl methylcellulose-g-poly (acrylamide)/LAPONITE® RD nanocomposites as novel magnetic-and pH-sensitive carriers for controlled drug release, RSC Adv. 5 (2015) 44516–44523.

[94] S. Punitha, R. Uvarani, A. Panneerselvam, S. Nithiyanantham, Physico-chemical studies on some saccharides in aqueous cellulose solutions at different temperatures–acoustical and FTIR analysis, J. Saudi Chem. Soc. 18 (2014) 657–665.

[95] B.W. Chieng, N.A. Ibrahim, W.M.Z.W. Yunus, M.Z. Hussein, Poly (lactic acid)/poly (ethylene glycol) polymer nanocomposites: effects of graphene nanoplatelets, Polymers 6 (2014) 93–104.

[96] S.N. Alhosseini, F. Moztarzadeh, M. Mozafari, S. Asgari, M. Dodel, A. Samadikuchaksaraei, S. Kargozar, N. Jalali, Synthesis and characterization of electrospun polyvinyl alcohol nanofibrous scaffolds modified by blending with chitosan for neural tissue engineering, IJN 7 (2012) 25.

[97] A. Kharazmi, N. Faraji, R.M. Hussin, E. Saion, W.M.M. Yunus, K. Behzad, Structural, optical, opto-thermal and thermal properties of ZnS–PVA nanofluids synthesized through a radiolytic approach, Beilstein J. Nanotechnol. 6 (2015) 529–536.

[98] C. Lustriane, F.M. Dwivany, V. Suendo, M. Reza, Effect of chitosan and chitosan-nanoparticles on post harvest quality of banana fruits, J. Plant Biotechnol. 45 (2018) 36–44.

[99] P.-P. Zuo, H.-F. Feng, Z.-Z. Xu, L.-F. Zhang, Y.-L. Zhang, W. Xia, W.-Q. Zhang, Fabrication of biocompatible and mechanically reinforced graphene oxide-chitosan nanocomposite films, Chem. Cent. J. 7 (2013) 1–11.

[100] K. Shameli, M. Bin Ahmad, S.D. Jazayeri, S. Sedaghat, P. Shabanzadeh, H. Jahangirian, Y. Abdollahi, Synthesis and characterization of polyethylene glycol mediated silver nanoparticles by the green method, Int. J. Mol. Sci. 13 (2012) 6639–6650.

[101] A. Ameri, G. Sodeifian, S.A. Sajadian, Lansoprazole loading of polymers by supercritical carbon dioxide impregnation: impacts of process parameters, J. Supercrit. Fluids 164 (2020) 104892.

[102] V. Pshezhetskii, A. Rakhnyanskaya, I. Gaponenko, Y.E. Nalbandyan, A differential scanning calorimetry study of polyvinyl alcohol, Polym. Sci. USSR 32 (1990) 722–726.

[103] S.C. Dey, M. Al-Amin, T.U. Rashid, M. Sultan, M. Ashaduzzaman, M. Sarker, S. Shamsuddin, Preparation, characterization and performance evaluation of chitosan as an adsorbent for remazol red, Int. J. Latest Res. Eng. Technol. 2 (2016) 52–62.

[104] F. Vozzi, T. Nardo, I. Guerrazzi, C. Domenici, S. Rocchiccioli, A. Cecchettini, L. Comelli, G. Vozzi, C. De Maria, F. Montemurro, Integration of Biomechanical and biological characterization in the development of porous poly (caprolactone)-based membranes for abdominal wall hernia treatment, Int. J. Polym. Sci. 2018 (2018) 1–15.